Hemorheology: Non-Newtonian Constitutive Models for Blood Flow Simulations

Adélia Sequeira

Abstract Experimental studies over many years have shown that blood flow exhibits non-Newtonian characteristics such as shear-thinning, viscoelasticity, yield stress and thixotropy. The complex rheology of blood is influenced by numerous factors including plasma viscosity, hematocrit and in particular, the ability of erythrocytes to form aggregates when at rest or at low shear rates and to deform at high shear rates, storing and releasing energy. Hemodynamic analysis of blood flow in vascular beds and prosthetic devices requires the rheological behavior of blood to be characterized by phenomenological constitutive equations relating the stress to the rate of deformation and flow. The objective of this chapter is to present a short overview of some macroscopic constitutive models that can mathematically characterize the rheology of blood and describe their known phenomenological properties. Some test cases formulated in idealized and anatomically realistic vessels will be considered to investigate the impact of the most significant non-Newtonian characteristics of blood on its flow behavior, based on numerical simulations of different blood constitutive equation under given sets of physiological flow conditions.

1 Introduction

Rheology is the science of the flow and deformation behavior of solid or fluid materials, including liquids and gases. This field deals with the theoretical notions of kinematics and dynamics, conservation laws and constitutive equations, describing the cross links between force, deformation and flow. It is also considered to be the study of stress-strain relationship in materials. When rheology is applied to the

A. Sequeira (✉)
Department of Mathematics, Instituto Superior Técnico, ULisboa, Center for Computational and Stochastic Mathematics - CEMAT, Lisboa, Portugal
e-mail: adelia.sequeira@math.tecnico.ulisboa.pt

A. Farina et al. (eds.), *Non-Newtonian Fluid Mechanics and Complex Flows*,
Lecture Notes in Mathematics 2212, https://doi.org/10.1007/978-3-319-74796-5_1

analysis of the properties of blood flow and its formed cellular elements it is called *hemorheology*. It involves the investigation of the macroscopic bulk properties of blood, determined in rheometric experiments, and its microscopic properties *in vitro* and *in vivo* (e.g. [129]). It also includes interactions among blood cellular components and between these components and endothelial cells that line blood vessels (microhemorheology).

The unceasing progress in the field of hemorheology is derived from its clinical interest since many cardiovascular diseases have their primary cause in blood flow pathologies. On the other hand, hemorheological abnormalities can be considered as a result (or a sign) of insufficient circulatory function. Basically, pathologies with hematological origin like leukemia, hemolytic anemia, thalassemia or pathologies associated with the risk factors of thrombosis and atherosclerosis like myocardial infarction, hypertension, strokes or diabetes are mainly related to disturbances of local homeostasis. For instance, small size lesions that may occur spontaneously in blood vessels due to endothelial injuries are quite common in small vessels. They can result in internal bleeding, infections or irreversible malfunction in the microcirculation (for example in the brain) and can lead to death. Cardiovascular diseases, including microcirculatory or macrocirculatory disorders are major causes of morbidity and mortality in developed countries and constitute a significant part of total health costs.

Human blood accounts for about 8% of total body weight, averaging 5200 ml. The circulatory system forms a closed loop for the flow of blood that achieves important functions, carrying oxygen, nutrients and various substances from the lungs to the tissues of the body and carbon dioxide back to the lungs, removing waste products of cells metabolism. Blood also plays a key role as a immune protection against foreign bodies (see e.g. [121]). The circulatory system consists of two separate parts, the systemic circulation and the pulmonary circulation, connected by the heart, a complex organ that acts like a pump to maintain a constant flow and is affected by the rest of the circulatory system. Oxygenated blood from the lungs is pumped by the left heart through the pulmonary veins into the systemic arteries, which form a tree of progressively smaller vessels, beginning with the aorta, branching to the small arteries, then to the arterioles and finally to the capillaries, where the exchange of gases takes place. Leaving the capillaries, the blood enters the systemic veins, through which it flows in vessels of progressively increasing size toward the right heart. The systemic veins consist of venules, small veins and the vena cava. The right heart pumps blood into the pulmonary arteries, which form a tree that distributes blood to the lungs, where blood leaves carbon dioxide and is purified with oxygen (e.g. [120]). A representation of the human circulatory system is shown in Fig. 1.

There are significant quantitative differences in pressure and blood volume, between the pulmonary and systemic circuits, but the output of the right and left sides of the heart must be in equilibrium. Veins are low pressure vessels with a low flow and their vessel walls are thin, in contrast to arteries. Table 1 (see [38]) displays average dimensions collected from different sources (Gabe et al. [46], Mao et al. [79], Feher [40], Caro et al. [24], Fung [45], Guyton [55], Gregg [54]),

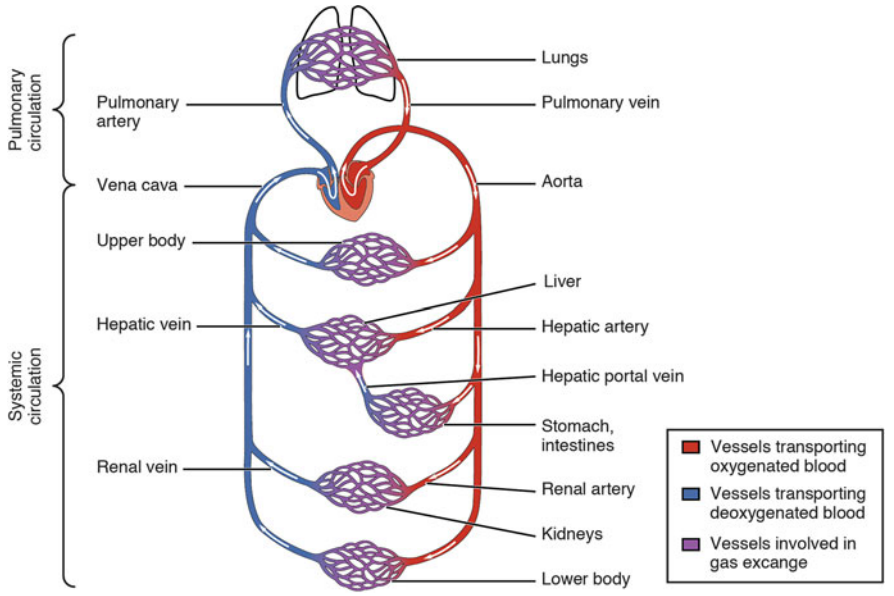

Fig. 1 Circulatory system diagram [Anatomy & Physiology, OpenStax College]

Table 1 Systemic circulation: average physiological parameters

Vessel	Nr.	Diam. (cm)	Cross-sectional area (cm^2)	Wall thickness (cm)	Mean pressure (kPa)	Mean velocity (cm/s)
Aorta	1	3	7	2×10^{-1}	12.5	12
Arteries	8×10^3	10^{-1}	8×10^{-3}	10^{-1}	12	45
Arterioles	10^7	5×10^{-3}	2×10^{-5}	2×10^{-3}	7	5
Capillaries	10^{10}	8×10^{-4}	5×10^{-7}	10^{-4}	3	0.1
Venules	4×10^7	10^{-2}	7.9×10^{-5}	2×10^{-4}	1.5	2
Veins	8×10^3	1.8×10^{-1}	10^{-1}	5×10^{-2}	1	10
Venae cavae	2	3	6	0.15	0.5	14

McDonald [82]). It is quite difficult to find complete and coherent parameters of this type when we compare all data provided by the different authors (see also e.g. [94, 122, 123]). In fact, all data concerning human blood are subjected to large variations, according to sex, body weight, and health conditions.

Despite the research and development efforts of many laboratories around the world, no blood substitute has yet been developed that can carry out the essential functions that whole blood performs in the circulatory system, and most specially for delivery and exchange in the microcirculation. Clearly there is a need for a better understanding of the special characteristics of blood and its flow properties. Therefore, together with laboratory trials, the mathematical and numerical study of

constitutive models that can capture the rheological response of blood over a range of flow conditions is ultimately recognised as an important tool for clinical diagnosis and therapeutic planning (see e.g. [33, 76]).

The aim of this chapter is to present an overview of the rheological properties of blood and its formed cellular elements, including the non-Newtonian characteristics of blood, and discuss some of the phenomenological macroscopic constitutive models that have been proposed in the literature to capture these properties. Moreover, in order to investigate the influence of the most significant non-Newtonian effects on blood flow behavior, some numerical test cases will be considered.

A review of blood rheology and of some of the most relevant constitutive models for blood can be found in e.g. [108, 109]. For a concise historical background about the development of hematology from the antiquity to the nineteenth century, see [38].

2 Blood Rheology

2.1 Blood Components

Blood is a concentrated heterogeneous suspension of several formed cellular elements, the *blood cells* or *hematocytes*, red blood cells (RBCs or *erythrocytes*), white blood cells (WBCs or *leukocytes*) and platelets (*thrombocytes*), in an aqueous polymeric and ionic solution (mainly Na^+, K^+, Ca^{2+} and CI^-), the *plasma*. Plasma represents ∼55% of the blood volume and is composed of ∼92% water and ∼3% particles, namely, electrolytes, organic molecules, numerous proteins (albumin, globulins and fibrinogen) and waste products. Plasma represents ∼55% of the blood volume and its central physiological function is to transport these dissolved substances, nutrients, wastes and the formed cellular elements throughout the circulatory system.

Normal erythrocytes are biconcave discs with a typical diameter of 6–8 μm and a maximal thickness of 1.9 μm [75]. In mammals these cells are non-nucleated and consist of a concentrated hemoglobin solution enveloped by a highly flexible membrane. The average volume of an erythrocyte is 90 μm^3 ([24]). Their number per cubic millimetre of blood is approximately 5 to 6 $\times$ 10^6 and they represent approximately 40 to 45% by volume of the normal human blood and more than 99% of all blood cells. The first percentage is called *hematocrit*. The primary function of erythrocytes is to transport oxygen and carbon dioxide carrying hemoglobin and a small portion of carbonic anhydrase, which catalyzes the reversible formation of carbonic acid from carbon dioxide and water.

Leukocytes are roughly spherical and much larger than erythrocytes, but they exist in a smaller number in blood: their diameter ranges between 6 and 17 μm and there are approximately 7 to 11 $\times$ 10^3 per cubic millimetre in a normal adult. Leukocytes are subdivided into main classes: granulocytes (65%) and agranulo-

cytes, comprising lymphocytes (30%), monocytes (5%) and natural killer cells. Granulocytes are further subdivided into neutrophils (95%), eosinophils (4%) and basophils (1%). The leukocytes maintain adhesion to the endothelium through rolling and play a vital role in fighting infection and thus are able to migrate out of the blood vessels and into the tissues. They have a slight influence on the rheology of blood, except in the capillaries or in disease states. For a better understanding of leukocytes biomechanical behavior, see e.g. [9, 34, 69, 72, 113]).

Thrombocytes are small discoid non-nucleated cell fragments, much smaller than erythrocytes and leukocytes, having a diameter 2–4 μm (and approximately 2–3 μm^3 in volume). Despite their smallness, thrombocytes (platelets) can perform an incredible number of actions, interacting with the environment by means of a rich array of receptors on their membrane and they are a vital component of the blood clotting mechanism. Blood coagulation is an extremely complex biological process in which blood forms clots (*thrombus*) to prevent bleeding (*hemostasis*); it is followed by their dissolution (fibrinolysis) and the subsequent repair of the injured tissue. The process involves large sequences of chemical reactions of complicated nature (*cascades*) and different interactions between the plasma, the vessel wall and activated thrombocytes (platelets), with a huge impact of the flowing blood on the resulting fibrin-platelets thrombus production and growth. There is a large number of books and review chapters on hemostasis (see e.g. [20, 38, 39, 66, 80, 135] and the references cited therein.

The total volume concentration of leukocytes and thrombocytes is only about 1%. All these cells are deformable but erythrocytes undergo a higher deformation, in particular when they pass through the capillaries. Deformations occur through a rearrangement of the cytoskeleton that supports cells shape avoiding rupture of the cell membranes.

Blood cells are continuously produced by the bone marrow over a human's life and they all reach ultimate maturity via a process called *hematocytopoiesis*. For example, erythrocytes have an average lifetime of 120 days and the body must produce about 3×10^9 new erythrocytes for each kilogram of body weight every day. Due to ageing and rupturing they must be constantly replaced (see e.g. [65]).

2.2 Non-Newtonian Properties of Blood

The non-Newtonian behavior of blood is largely due to three characteristics of RBCs: their ability to form aggregates when at rest or at low shear rates, their general distribution in the flowing plasma, namely the ability of these 3D microstructures to deform and store energy and their tendency to align in the flow direction, at high shear rates (e.g. [29, 111]). The high deformability of RBCs is due to the absence of a nucleus, to the elastic and viscous properties of its membrane and also to geometric factors such as the shape, volume and membrane surface area [27].

Rheometers are precision instruments applied to measure wide ranges of stress, strain, and strain rate of a material. The following kinds of rheometers are the

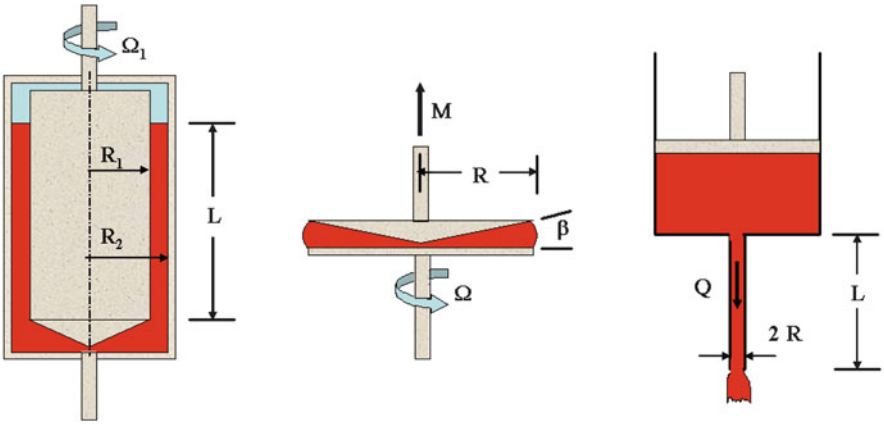

Fig. 2 Representation of the three mostly used rheometers in blood measurements (from [109])

mostly used to measure blood flow properties: the concentric cylindrical rheometer (Couette rheometer), the cone and plate rheometer and the capillary rheometer, Fig. 2. In the Couette rheometer, blood is placed in the annulus between two concentric cylinders and it's motion is driven by the rotation of one or both cylinders; In the cone and plate rheometer, blood is loaded between the cone and the plate and driven by the rotation of the cone; the capillary rheometer is of simple use and the test fluid is driven by gravity, compressed gas or a piston from a reservoir through a cylinder rigid tube. These rheometers can be used to obtain approximate measurements of viscometric and viscoelastic material functions (see e.g [109]).

As discussed below, it has been experimentally verified that the response of RBCs in shear flows undergoes three flow regimes: at low shear rates, in the presence of fibrinogen and large globulins (proteins found in plasma) erythrocytes form a complex three dimensional microstructure (*rouleaux*), while at high shear rates, this microstructure is lost and flow induced radial migration may lead to a non-homogeneous distribution of erythrocytes. A transition in microstructure is found between these two regimes.

To better analyze the experimental data on blood it is helpful to explore the literature on the rheology of particle suspensions. For rigid particles, a vast amount of published literature exists (see e.g. [35, 110]). However, the study of suspensions of multiple, interacting and highly deformable particles such as blood, has received less attention and presents a challenge for researchers in both theoretical and computational fluid dynamics.

2.2.1 Viscosity of Blood

Here we refer to the *apparent viscosity* of blood (or, more generally of a non-Newtonian fluid, independently of the specific rheological model), as the quantity

measured by a viscometer, for shear rates in the expected natural range. This is approximately an average measure of the fluid resistance to flow. The expression *relative viscosity* is also used for blood, denoting the ratio of the suspension viscosity (apparent viscosity) to the viscosity of the suspending fluid (plasma). Commonly used viscosity units are: *poise* (*P*), *centipoise* (*cP*), which is 0.01 P and pascal-second (*Pa s*), the SI unit of viscosity equivalent to Newton-second per square metre ($N\,s/m^2$). One poise is exactly 0.1 Pa s.

Usually blood has higher viscosity than plasma, and when the hematocrit rises, the viscosity of the suspension increases and the non-Newtonian behavior of blood becomes more relevant, in particular at very low shear rates. As mentioned above, for blood at rest or at very low shear rates the erythrocytes have the ability to form a primary aggregate structure of rod shaped stacks of individual cells (rouleaux), that align to each other and form a secondary structure consisting of branched three-dimensional (3D) aggregates [112]. The apparent viscosity (measured by a viscometer) increases slowly until a shear rate less than $1\,s^{-1}$, and then it increases significantly [24]. It has been experimentally observed that rouleaux will not form if the erythrocytes have been hardened or in the absence of fibrinogen and globulins [28]. In fact, suspensions of erythrocytes in plasma demonstrate a strong non-Newtonian behavior whereas when they are in suspension in physiological saline (with no fibrinogen or globulins) the behavior of the fluid is Newtonian [32, 85]. For standing blood subjected to a shear stress lower than a critical value, these 3D structures resist to flow until a certain force is applied and blood exhibits a yield stress behavior. This can happen only if the hematocrit is high enough. The existence of yield stress for blood will be discussed below (see Sect. 2.2.2).

At moderate to high shear rates, RBCs are dispersed in the plasma and the properties of the blood are influenced by their tendency to align and form layers in the flow, as well as by their deformation. The effect of RBC deformability on the viscosity of suspensions was clearly described in [28].

For shear rates above $400\,s^{-1}$, erythrocytes lose their biconcave shape, become fully elongated and are transformed into ellipsoids with major axes parallel to the flow direction. The tumbling of the erythrocytes is absent, there are almost no collisions, and their contours change according to the tank-trading motion of the cells membranes about their interior. The apparent viscosity decreases and this becomes more evident in smaller than in larger vessels. This happens with vessels of internal diameter less than 1 mm and it is even more pronounced in vessels with a diameter of 100–200 μ m. The geometric packing effects and radial migration of erythrocytes can act to lower the hematocrit adjacent to the vessel wall and contribute to decrease the blood viscosity. This is known as the *Fåhraeus–Lindqvist* effect, [41, 42]. *Plasma skimming* is another effect that results in diminishing the viscosity when blood flows into small lateral vessels compared with the parent vessel.

As a consequence of this behavior we can say that one of the most important non-Newtonian characteristics of blood is the shear-thinning viscosity. This happens in small size vessels or in regions of stable recirculation, like in the venous system and parts of the arterial vasculature where geometry has been altered and erythrocyte

aggregates become more stable, like downstream a stenosis or inside a saccular aneurysm. However, in most parts of the arterial system, blood flow is Newtonian in normal physiological conditions.

Numerous techniques have been developed to quantify erythrocytes aggregation in a flow field, with applications to *in vitro* flow models or to *in vitro* microvascular measurements.These include estimates of aggregate size from direct measurements, Fourier analysis of spatial variation in light intensity, analysis of transmitted and reflected light, and measurement of the light scattering properties of RBCs (see e.g. [15, 51, 93, 96]).

Experiments on blood at low shear rates are very difficult to perform and there remains a controversy over the blood flow behavior in the limit of shear rate tending to zero. Figure 3 displays the shear-thinning behavior of whole blood as experimentally observed by Chien et al. [28]. Each of these data points represents an equilibrium value obtained at a fixed shear rate.

In addition, it is important to point out that, like in many other liquids, the viscosity of whole blood is also strongly dependent on temperature and, when comparing blood viscosity data from different sources, the temperature at which data was obtained must be considered. The dependence of blood viscosity on temperature is similar to that of water for temperatures ranging from 10 °C to 40 °C and shear rates from 1 to 100 s^{-1}[84]. The variation of plasma temperature follows approximately that of water [25] and, consequently, blood viscosity is often related to plasma or water viscosity, at the same temperature.

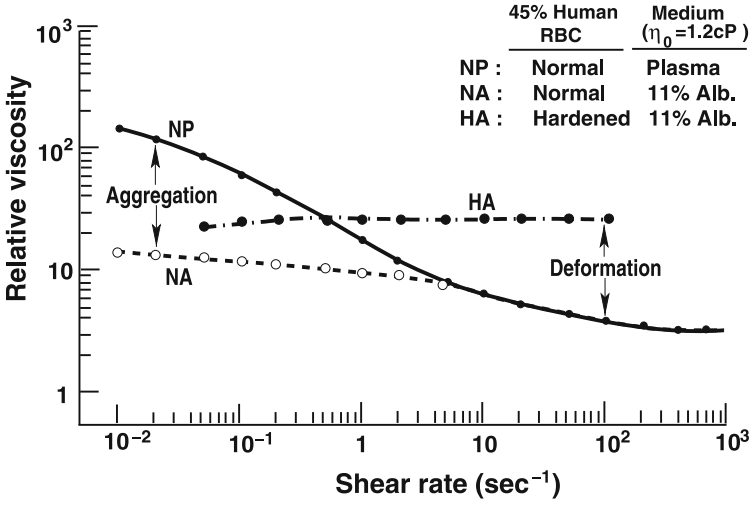

Fig. 3 Variation of the relative viscosity as a function of the shear rate for normal RBC in heparinised plasma (NP), normal RBC in albumin-Ringer solution (NA) and hardened RBCs in albumin-Ringer solution (HA) at a temperature of 37°C, hematocrit $Ht = 45\%$ using a Couette viscometer (reproduced from [28])

2.2.2 Yield Stress of Blood

Some bodies, like pastes, do not deform when the shear stress is below a critical value, while they start flowing like a fluid if the stress exceeds that threshold. The phenomenon is explained by the rupture of inner bonds. Systems with an yield stress are called Bingham fluids [14]. This critical stress level, called the yield value or yield, is typically treated as a constant material property of the fluid. An extensive description of methods for measuring yield stress is given in [89, 92].

Blood also demonstrates yield stress although there is a controversy about this issue. Reported values for the yield stress of blood have a great variation ranging from 0.002 to 0.40 dynes/cm^2, see e.g. [32]. This variation has been attributed to artifacts arising from interactions between the erythrocytes and surfaces of the rheometer as well as to the experimental methods used to measure the yield stress and the length of time over which the experiments are run [11]. Rather than treating the yield stress as a constant, it should be considered as a function of time and linked to thixotropy, as later proposed by other researchers [88]. Some studies have indicated that yield stress is correlated to the hematocrit level and to the concentration of fibrinogen in blood plasma. When the hematocrit level falls below a critical level, the yield stress characteristic of blood becomes negligible [83].

2.2.3 Viscoelasticity and Thixotropy of Blood

Viscoelastic fluids are viscous fluids which have the ability to store and release energy. The viscoelasticity of blood at normal hematocrits is primarily attributed to the reversible deformation of the RBCs 3D microstructures [30, 128]. Elastic energy is due to the properties of the RBC membrane which exhibits stress relaxation [36, 119] and the bridging mechanisms within the 3D structure. Moreover, the experimental results of Thurston [124] have shown that the relaxation time depends on the shear rate. Thurston was the first to measure the viscoelastic properties of blood and the dependence of blood viscoelasticity on factors such as temperature, hematocrit and RBC properties. He has contributed to most of the experimental work developed in this area (see [128] and the references cited therein).

The viscoelastic effects in blood circulation are magnified by its pulsatile nature and by the elastic properties of the blood vessels and the porous tissue through which blood is transported [23] and there is an interaction between the viscoelastic behavior of blood with that of the vessel wall and porous tissue.

In view of the available experimental evidence, it is reasonable to develop non-Newtonian fluid models for blood that are capable of shear-thinning and stress relaxation, with the relaxation time depending on the shear rate. To date, very little is known concerning the response of such fluids. In fact, viscoelastic properties are of relatively small magnitude and they have generally only been measured in the context of linear viscoelasticity. By shear rates of the order of $10\,s^{-1}$ the elastic nature of blood is negligible as evidenced by a merging of the oscillatory and steady flow viscosities. However, if viscoelastic constitutive equations are used

to model blood in the circulatory system in higher shear rates conditions, the finite viscoelastic behavior of blood should be considered. Viscoelastic constitutive models for blood will be discussed below (see Sect. 2.3.4).

Another important non-Newtonian property of blood closely related to shear-thinning, is the thixotropic behavior, essentially due to the finite time required for the formation and dissolution of the 3D aggregates of erythrocytes. Indeed, the build-up and breakdown of the 3D microstructures, their elongation and recovery, and the formation and breakdown of layers of the aligned erythrocytes evolve in a finite time, and these processes can play an important role in blood rheometry [11]. There is a large variety of published definitions for thixotropy, in the fields of industrial or biological applications. The following definition can be found in [12]: "When a reduction in magnitude of rheological properties of a system, such as elastic modulus, yield stress, and viscosity, for example, occurs reversibly and isothermally with a distinct time dependence on application of shear strain, the system is described as *thixotropic*". Fluids whose behavior is opposite to thixotropic fluid (i.e. thickening under stress) are called *rheopectic*.

Thixotropy is more pronounced at low shear rates with a long time scale. The effect in blood flow is less pronounced than other non-Newtonian effects [78] and this can explain the limited studies devoted to this property.

It should be emphasized that most of the reported non-Newtonian properties and rheological parameters of blood are obtained *in vitro*, as indicators of *in vivo* real measurements. Experimenting with blood out of the body can find many obstacles. The simple process of extracting blood may apply high stresses, altering the original rheological properties. Then partial coagulation, particularly in the absence of flow, can severely influence the values of viscosity, viscoelastic or yield stress parameters. Moreover, the consistency of these approximations depends on the information about experimental and individual conditions. Complementary studies of sensitivity analysis and uncertainty quantification should be performed, especially when those values are used for patient-specific modeling and simulations.

2.3 Constitutive Models for Blood

The mechanical properties of blood should be studied by considering a fluid containing a suspension of particles. A fluid is said to be Newtonian if it satisfies the Newton's law of viscosity (the shear stress is proportional to the rate of shear and the viscosity is the constant of proportionality). Blood plasma, which consists mostly of water, is a Newtonian fluid. However, the whole blood has complex mechanical properties which become particularly significant when the particles size is much larger, or at least comparable, with the lumen size. In this case, which happens at the microcirculation level (in the small arterioles and capillaries) blood cannot be modelled has a homogeneous fluid and it is essential to consider it as a suspension of blood cells (specially erythrocytes) in plasma. The presence of the blood cellular elements and their interactions leads to significant changes in the blood rheological

properties and reliable measurements need to be performed to derive appropriate microstructural models (see e.g. [101, 115, 134]).

Blood is a non-Newtonian fluid, but it can however be regarded as Newtonian depending on the size of the blood vessels and the flow behavior, as in arteries with diameters larger than 100 μ m where measurements of the apparent viscosity show that it ranges from 0.003 to 0.004 Pa s and the typical Reynolds number is about 0.5.

Here we assume that all macroscopic length and time scales are sufficiently large compared to length and time scales at the level of an individual erythrocyte so that the continuum hypothesis holds. Thus the models presented here are not appropriate in the capillary network. For an overview of hemorheology in the microcirculation we refer the reader to the review article of Popel and Johnson [101], as already referred.

2.3.1 Constant Viscosity Models

As a first step towards the macroscopic modeling of blood flow we consider the most general form of constitutive equations for incompressible viscous fluids, defining the Cauchy stress tensor $\mathbf{T}$ such that

$$\mathbf{T} = -p\mathbf{I} + \boldsymbol{\tau}, \tag{1}$$

where p (pressure) is the Lagrange multiplier arising from the incompressibility constraint, $\mathbf{I}$ is the identity matrix and $\boldsymbol{\tau}$ is the *extra-stress* (or deviatoric stress) tensor, representing the forces which the material develops in response to being deformed.

In large vessels normal blood has a *Newtonian* behavior, meaning that the extra-stress is proportional to the symmetric part of the velocity gradient,

$$\boldsymbol{\tau} = 2\mu\mathbf{D}(\mathbf{u}), \tag{2}$$

where μ is the (constant) dynamic viscosity of blood and the tensor $\mathbf{D}(\mathbf{u}) \equiv \mathbf{D} = (\nabla\mathbf{u} + \nabla\mathbf{u}^T)/2$ is the symmetric part of the velocity gradient (rate of deformation or strain rate) [118]. Taking into account the principles of conservation of linear momentum and conservation of mass (reduced to a divergence-free constraint) for isothermal incompressible flows, the substitution of $\boldsymbol{\tau}$ given by (2) in the Cauchy stress equation (1) leads to the system

$$\begin{cases} \rho\dfrac{\partial\mathbf{u}}{\partial t} + \rho(\mathbf{u}\cdot\nabla)\mathbf{u} = -\nabla p + \nabla\cdot 2\mu\mathbf{D}(\mathbf{u}), \\ \nabla\cdot\mathbf{u} = 0, \end{cases} \tag{3}$$

where $\mathbf{u}$ and p denote the blood velocity and pressure, with $t \geq 0$ and ρ is the blood density.

In this case, since μ is constant, from the continuity equation we obtain

$$\nabla \cdot [\mu(\nabla \mathbf{u} + \nabla \mathbf{u}^T)] = \mu(\Delta \mathbf{u} + \nabla \nabla . \mathbf{u}) = \mu \Delta \mathbf{u}$$

and system (3) is written in form

$$\begin{cases} \rho \dfrac{\partial \mathbf{u}}{\partial t} - \mu \Delta \mathbf{u} + \rho(\mathbf{u} \cdot \nabla)\mathbf{u} + \nabla p = 0, \\ \nabla \cdot \mathbf{u} = 0. \end{cases} \tag{4}$$

These are the well-known incompressible Navier-Stokes (NS) equations (proposed by **Navier** in 1822 and later by **Stokes** in 1845). Here $\rho(\mathbf{u} \cdot \nabla)\mathbf{u}$ is the nonlinear convective term and $\nabla \cdot [\mu(\nabla \mathbf{u} + \nabla \mathbf{u}^T)]$ is the diffusion term showing the role of viscosity in propagating momentum. In the larger arteries and veins there is a predominance of inertial effects over the viscous ones. System (4) must be closed with appropriate initial and boundary conditions.

The NS equations can also be rescaled and written in a non-dimensional form by introducing the following quantities:

$$x = \frac{\tilde{x}}{R}, \qquad t = \frac{U\tilde{t}}{R}, \qquad p = \frac{\tilde{p}R\mu}{U},$$

where the symbol $\tilde{}$ is attached to dimensional parameters (R represents a reference length—the radius of the vessel, U is a characteristic velocity—the mean blood flow velocity). We also introduce the important dimensionless quantity used in fluid mechanics, the *Reynolds number—Re* defined as $Re = \frac{\rho UR}{\mu}$, that means the ratio of momentum forces to viscous forces, and quantifies the relation between these two forces for given flow conditions. More precisely, the NS equations can be written in a simplified form as

$$\begin{cases} Re\left(\dfrac{\partial \mathbf{u}}{\partial t} + (\mathbf{u} \cdot \nabla)\mathbf{u}\right) - \Delta \mathbf{u} + \nabla p = 0, \\ \nabla \cdot \mathbf{u} = 0. \end{cases} \tag{5}$$

When $Re \ll 1$ (for instance blood flow in smaller arteries), we may neglect the convective term compared to the viscous contribution. Then blood could be modeled by the simpler Stokes equations (creeping flow or Stokes flow). However, as already mentioned, in the smaller arteries the non-Newtonian behavior of blood becomes relevant. On the other hand, when $Re \gg 1$ (*high Reynolds number flows*) the flow becomes unstable. In normal physiological conditions instabilities can occur in some vascular regions, in particular in the systolic phase at the exit of the aortic valve or in bifurcations, but normally there is no time for the flow to develop turbulence. In pathological conditions, like in case of severe anaemia (low blood viscosity) or due to the presence of a stenosis (stenotic artery), the transition from laminar to turbulent flow can occur [44]. Such conditions are nevertheless rare and consequently turbulent flow models are not used in cardiovascular modeling and simulations.

From the analytical and numerical view points the Navier-Stokes system with appropriate initial and boundary conditions has been the object of intensive research, but there are still important issues to be solved. In the mathematical theory, we emphasize the famous global in time uniqueness in 3D, related to the regularity of solution. (see e.g. [47, 48]).

Since the pioneering work of Perktold in the late 1980s and early 1990s [97, 98], much of the research in modeling blood flow in the human arterial system has focused on the numerical solution of the 3D Navier-Stokes system which provides hemodynamic factors like blood flow velocity and pressure fields, and wall shear stress (WSS) or the wall compliance (e.g. [99, 100]), difficult to extract using simpler models and experimental measurements.

2.3.2 Generalized Newtonian Models

As already discussed, this set of equations is commonly used to describe blood flow in healthy arteries. However, under certain experimental or physiological conditions, particularly at low shear rates, blood exhibits relevant non-Newtonian characteristics and more complex constitutive models need to be used. In this case, we require a more general constitutive equation relating the state of stress to the rate of deformation. It can be shown that the most general model of the form (1) with $\boldsymbol{\tau} = \boldsymbol{\tau}(\nabla \mathbf{u})$, satisfying invariance requirements, can be written as [10]

$$\boldsymbol{\tau} = \phi_1(\mathrm{II}_{\mathbf{D}}, \mathrm{III}_{\mathbf{D}})\mathbf{D}(\mathbf{u}) + \phi_2(\mathrm{II}_{\mathbf{D}}, \mathrm{III}_{\mathbf{D}})\mathbf{D}(\mathbf{u})^2 \tag{6}$$

where $\mathrm{II}_{\mathbf{D}}$ and $\mathrm{III}_{\mathbf{D}}$ are the second and third principal invariants of the rate of deformation tensor $\mathbf{D} = \mathbf{D}(\mathbf{u})$. These invariants are given by

$$\mathrm{II}_{\mathbf{D}} = 1/2\,((\mathrm{tr}\,\mathbf{D}(\mathbf{u}))^2 - \mathrm{tr}\,(\mathbf{D}(\mathbf{u}))^2), \qquad \mathrm{III}_{\mathbf{D}} = \det(\mathbf{D}(\mathbf{u})). \tag{7}$$

where $t\mathrm{tr}\,\mathbf{D} = \mathrm{I}_{\mathbf{D}} = 0$ for divergence free velocity fields, essential for incompressible fluids (isochoric motions). To simplify the notation, from now on $\mathbf{D}(\mathbf{u})$ will be replaced by $\mathbf{D}$,

Incompressible fluids of the form (6) are typically called *Reiner-Rivlin fluids*. We remark that the presence of ϕ_2 in (6) is necessary to match experimental results on "real" fluids and the dependence on the value of II_D is often neglected [10].

Therefore, attention is particularly given to a special class of Reiner-Rivlin fluids called *generalized Newtonian fluids*, for which

$$\boldsymbol{\tau} = 2\mu(\mathrm{II}_{\mathbf{D}}, \mathrm{III}_{\mathbf{D}})\mathbf{D}, \tag{8}$$

Since for "real" fluids $\mathrm{III}_{\mathbf{D}}$ is identically zero and $\mathrm{II}_{\mathbf{D}}$ is not a positive constant, it is useful to introduce a measure of the rate of deformation, the *shear rate* denoted by $\dot{\gamma}$ and defined by

$$\dot{\gamma} = \sqrt{2\,\mathrm{tr}\,(\mathbf{D}^2)} = \sqrt{-4\,\mathrm{II}_{\mathbf{D}}}. \tag{9}$$

and write the stress tensor for the generalized Newtonian model (8) in the form

$$\boldsymbol{\tau} = 2\mu(\dot{\gamma})\mathbf{D}, \tag{10}$$

where $\mu(\dot{\gamma})$ is a shear dependent viscosity function.

A simple example of a generalized Newtonian fluid is the *power-law* fluid, for which the viscosity function is given by

$$\mu(\dot{\gamma}) = K\,\dot{\gamma}^{n-1}, \tag{11}$$

the positive constants n and K being the power-law index and the consistency, respectively. This model includes, as a particular case, the constant viscosity fluid (Newtonian) when $n = 1$. For $n < 1$ it leads to a monotonic decreasing function of the shear rate (shear-thinning fluid) and for $n > 1$ the viscosity increases with shear rate (shear thickening fluid). The shear-thinning power-law model is often used for blood, due to the analytical solutions easily obtained for its governing equations, but there is a shortcoming since it predicts an unbounded viscosity at zero shear rate and zero viscosity when $\dot{\gamma} \to \infty$, which is unphysical.

One of the important extensions of the power-law model is due to Walburn and Schneck [133] who considered the dependence of the viscosity on the hematocrit (*Ht*) and total protein minus albumin (*TPMA*) in the constants n and K, based on nonlinear regression analysis, and found

$$K = C_1 exp(C_2 Ht), \qquad n = 1 - C_3 Ht. \tag{12}$$

According to Cho and Kensey [31] commonly used values in the literature for blood density ρ and for the asymptotic viscosities at zero and infinity shear rates μ_o and μ_∞, at 37 °C, are the following

$$\rho = 1056\,\mathrm{kg/m^3}, \qquad \mu_o = 0.056\,\mathrm{Pa\,s}, \qquad \mu_\infty = 0.00345\,\mathrm{Pa\,s}, \tag{13}$$

where the values of

$$\mu_0 = \lim_{\dot{\gamma}\to 0} \mu(\dot{\gamma}), \quad \mu_\infty = \lim_{\dot{\gamma}\to \infty} \mu_(\dot{\gamma}).$$

were obtained from a set of data including both human and canine blood and for hematocrits ranging from 33–45%.

Note that the values in (13) are only significant for theoretical constitutive models. In practice, the lower limit in shear rate at which viscosity can be measured is limited by experimental trials. The high shear rate limit has no real physical meaning and it is taken as the highest shear value.

As discussed earlier in this chapter (Sect. 2.2) the material parameters of blood are quite sensitive to the state of blood constituents as well as temperature [84].

Table 2 Material constants for power-law model obtained by various researchers using fit of (11) to human blood data at different hematocrits

Ht (%)	n	k	Source
40.5	0.828	0.009267	Kim et al. [67], 37 °C
35	0.8254	0.0880	Walburn and Schneck [133], 37 °C
40	0.8004	0.1147	
45	0.7755	0.1482	
45	0.61	0.42	Liepsch and Moravec [73], 23 °C

For comparison, results predicted from the Walburn-Schneck model (12) are shown

The dependence on hematocrit is included in material parameters for the power-law model that were obtained for human blood, Table 2. The corresponding viscosity functions are shown in Fig. 2. The viscosity functions obtained from [67] for $Ht = 40, 5\%$ and [133] for $Ht = 40\%$, are quite close. In contrast, those in [73] and [133] for $Ht = 45\%$ are substantially different, possibly due to the difference in temperatures.

Other viscosity functions with bounded and non-zero limiting values of viscosity can be written in the general form

$$\mu(\dot{\gamma}) = \mu_\infty + (\mu_0 - \mu_\infty)F(\dot{\gamma})$$

or, in non-dimensional form as

$$\frac{\mu(\dot{\gamma}) - \mu_\infty}{\mu_0 - \mu_\infty}.$$

Here, $F(\dot{\gamma})$ is a shear dependent function, satisfying the following natural limit conditions

$$\lim_{\dot{\gamma}\to 0} F(\dot{\gamma}) = 1, \quad \lim_{\dot{\gamma}\to \infty} F(\dot{\gamma}) = 0.$$

Different choices of the function $F(\dot{\gamma})$ correspond to different models for blood flow, with material constants quite sensitive and depending on a number of factors including hematocrit, temperature, plasma viscosity, age of erythrocytes, exercise level, gender or disease state (Fig. 4).

Table 3 includes some of the most common generalized Newtonian models that have been considered in the literature for the shear dependent viscosity of whole blood. Values for the material constants given in this table were obtained by Cho and Kensey[31]. As mentioned above those set of values were obtained for human and canine blood (Ht ranging from 33%–45%), using a nonlinear least squares analysis.

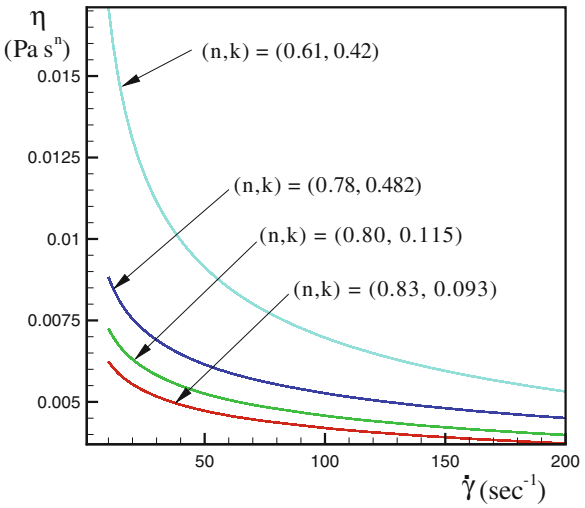

Fig. 4 Comparison of viscosity functions of $\dot{\gamma}$ for extensions of the power-law model (11) using material constants given by different authors (Table 2) obtained by curve fit to experiments

Table 3 Material constants for various generalized Newtonian models for blood with $\mu_0 = 0.056\,\text{Pa s}$, $\mu_\infty = 0.00345\,\text{Pa s}$

Model	$\frac{\mu(\dot{\gamma}) - \mu_\infty}{\mu_0 - \mu_\infty}$	Material constants for blood
Powell-Eyring	$\frac{\sinh^{-1}(\lambda\dot{\gamma})}{\lambda\dot{\gamma}}$	$\lambda = 5.383\,\text{s}$
Cross	$\frac{1}{1+(\lambda\dot{\gamma})^m}$	$\lambda = 1.007\,\text{s}$, $m = 1.028$
Modified cross	$\frac{1}{(1+(\lambda\dot{\gamma})^m)^a}$	$\lambda = 3.736\,\text{s}$, $m = 2.406$, $a = 0.254$
Carreau	$(1+(\lambda\dot{\gamma})^2)^{(n-1)/2}$	$\lambda = 3.313\,\text{s}$, $n = 0.3568$
Carreau-Yasuda	$(1+(\lambda\dot{\gamma})^a)^{(n-1)/a}$	$\lambda = 1.902\,\text{s}$, $n = 0.22$, $a = 1.25$

2.3.3 Yield Stress Models

Yield stress models can be useful to model blood flow in capillaries and some porous structures where flow at very low shear rates occurs. Yield stress materials require a finite shear stress $\boldsymbol{\tau}_Y$ (the yield stress) to start flowing. A relatively simple, and physically relevant yield criterion is given by

$$\sqrt{|\text{II}_{\boldsymbol{\tau}}|} = \boldsymbol{\tau}_Y, \tag{14}$$

where $\text{II}_{\boldsymbol{\tau}}$ is the second invariant of the extra stress tensor, $\boldsymbol{\tau}$ (defined in (7)). Therefore, for $\sqrt{|\text{II}_{\boldsymbol{\tau}}|} < \boldsymbol{\tau}_Y$, the fluid will not flow.

The most usual yield stress model for blood is the Casson model (e.g. [86, 114]) which, for simple shear flow, has the form

$$\begin{aligned} &\sqrt{|\mathrm{II}_{\boldsymbol{\tau}}|} < \boldsymbol{\tau}_Y \Longrightarrow \mathbf{D} = 0 \\ &\sqrt{|\mathrm{II}_{\boldsymbol{\tau}}|} \geq \boldsymbol{\tau}_Y \Longrightarrow \begin{cases} \mathbf{D} = \frac{1}{2\mu_N}\left(1 - \frac{\sqrt{\boldsymbol{\tau}_Y}}{\sqrt[4]{|\mathrm{II}_{\boldsymbol{\tau}}|}}\right)^2 \boldsymbol{\tau} \\ \boldsymbol{\tau} = 2\left(\sqrt{\mu_N} + \frac{\sqrt{\boldsymbol{\tau}_Y}}{\sqrt[4]{4|\mathrm{II}_{\mathbf{D}}|}}\right)^2 \mathbf{D}. \end{cases} \end{aligned} \tag{15}$$

The Newtonian constitutive equation is a special case of (15) for $\boldsymbol{\tau}_Y$ equal to zero, μ_N being the Newtonian viscosity. The Casson fluid behaves rigidly until the yield criterion (14) is verified, and after that it displays a shear-thinning behavior.

Other yield stress models used for blood are the Bingham model [102] given by

$$\begin{aligned} &\sqrt{|\mathrm{II}_{\boldsymbol{\tau}}|} < \boldsymbol{\tau}_Y \Longrightarrow \mathbf{D} = 0 \\ &\sqrt{|\mathrm{II}_{\boldsymbol{\tau}}|} \geq \boldsymbol{\tau}_Y \Longrightarrow \begin{cases} \mathbf{D} = \frac{1}{2\mu}\left(1 - \frac{\sqrt{\boldsymbol{\tau}_Y}}{\sqrt{|\mathrm{II}_{\boldsymbol{\tau}}|}}\right) \boldsymbol{\tau} \\ \boldsymbol{\tau} = 2\left(\mu + \frac{\boldsymbol{\tau}_Y}{2\sqrt{|\mathrm{II}_{\mathbf{D}}|}}\right) \mathbf{D}. \end{cases} \end{aligned} \tag{16}$$

where μ is the constant viscosity attained once the material flows, or the Herschel-Bulkley model (see e.g. [56]) which is similar to the Bingham model (16) which behaves as a power-law viscosity model once it begins to flow (μ in (16) is replaced by the power-law viscosity $\mu(\dot{\gamma}) = K\,\dot{\gamma}^{n-1}$, defined in (11)

$$\begin{aligned} &\sqrt{|\mathrm{II}_{\boldsymbol{\tau}}|} < \tau_Y \Longrightarrow \mathbf{D} = 0 \\ &\sqrt{|\mathrm{II}_{\boldsymbol{\tau}}|} \geq \boldsymbol{\tau}_Y \Longrightarrow \begin{cases} \mathbf{D} = \frac{1}{2K\,\dot{\gamma}^{n-1}}\left(1 - \frac{\sqrt{\boldsymbol{\tau}_Y}}{\sqrt{|\mathrm{II}_{\boldsymbol{\tau}}|}}\right) \boldsymbol{\tau} \\ \boldsymbol{\tau} = 2\left(K\,\dot{\gamma}^{n-1} + \frac{\boldsymbol{\tau}_Y}{2\sqrt{|\mathrm{II}_{\mathbf{D}}|}}\right) \mathbf{D}. \end{cases} \end{aligned} \tag{17}$$

Quemada [105] also developed a constitutive model suitable for blood, using an approach with the apparent viscosity μ given by

$$\mu(\dot{\gamma}) = \mu_F \left(1 - \frac{1}{2}\frac{k_0 + k_\infty\sqrt{\dot{\gamma}/\dot{\gamma}_c}}{1 + \sqrt{\dot{\gamma}/\dot{\gamma}_c}}\varphi\right)^{-2}, \tag{18}$$

where μ_F, φ and $\dot{\gamma}_c$ are the viscosity of the suspending fluid, the volume concentration of the dispersed phase and a critical shear rate, respectively. Table 4 provides material parameters for the Quemada and Casson models for blood used in [91].

Table 4 Material constants for Quemada (18) and Casson (15) models: $Ht = 45\%$ and temperature $T = 37\,^{\circ}\mathrm{C}$

Model	Material constants for blood
Quemada	$\mu_F = 1.2\,\mathrm{mPa\,s}$ $k_\infty = 2.07$ $k_0 = 4.33$ $\dot{\gamma}_c = 1.88\,\mathrm{s}^{-1}$ $\varphi = 0.45$
Casson	$\mu_N = 3.1\,\mathrm{mPa\,s}$

As discussed above, the existence of a yield stress and its use as a material parameter is still nowadays a controversial issue, due to the sensitivity of yield stress measurements.

2.3.4 Viscoelastic Models

There is a large number of *in vitro* experiments confirming that blood can store and dissipate energy during the aggregation of the erythrocytes and the distortion of the formed 3D microstructures (e.g. [30, 77, 125, 131]. As previously mentioned in Sect. 2.2.3, Thurston [124] was among the earliest to recognise the viscoelastic nature of blood and that the viscoelastic behaviour is less prominent with increasing shear rate. In view of the available experimental evidence, it is reasonable to develop non-Newtonian fluid models for blood that are capable of shear-thinning and stress relaxation, with the relaxation time depending on the shear rate.

None of the models already presented in the previous sections re able to capture the viscoelastic response of blood. One of the simplest quasi-linear rate-type viscoelastic models accounting for the viscoelasticity of blood is the Maxwell model

$$\boldsymbol{\tau} + \lambda_1 \frac{\delta \boldsymbol{\tau}}{\delta t} = 2\mu \mathbf{D}, \tag{19}$$

where λ_1 is the relaxation time and the operator $\delta(.)/\delta t$ stands for the so-called *upper-convected derivative* defined by

$$\delta \boldsymbol{\tau}/\delta t = \overset{\triangledown}{\boldsymbol{\tau}} =: \frac{D\boldsymbol{\tau}}{Dt} - \mathbf{L}\boldsymbol{\tau} - \boldsymbol{\tau}\mathbf{L}^T \tag{20}$$

with $\mathbf{L} = \nabla \mathbf{u} + \nabla \mathbf{u}^T =: 2\mathbf{D}$. This is a generalization of the material time derivative,

$$\frac{D\boldsymbol{\tau}}{Dt} = \frac{\partial \boldsymbol{\tau}}{\partial t} + \frac{\partial \boldsymbol{\tau}}{\partial \mathbf{x}} \frac{d\mathbf{x}}{dt}. \tag{21}$$

$\delta \boldsymbol{\tau}/\delta t$ is chosen to be objective under a superposed rigid body motion, meaning that it is frame indifferent or that the response of the material is not affected by its location and orientation. The resulting second-order tensor is symmetric [108].

A generalized Maxwell model that was applicable to one dimensional flow simulations was proposed by Thurston [127] who observed later that, beyond a critical shear rate, the nonlinear behavior is related to the microstructural changes that occur in blood. Thurston's work was suggested to be more applicable to venous or low shear unhealthy blood flow than to arterial flows. Recently, a generalized Maxwell model related to the microstructure of blood, inspired on the behaviour of transient networks in polymers, and exhibiting shear-thinning, viscoelasticity and thixotropy, has been derived by Owens [95].

A more general class of rate-type models, called Oldroyd type models, is defined by

$$\boldsymbol{\tau} + \lambda_1 \frac{\delta \boldsymbol{\tau}}{\delta t} = 2\mu(\mathbf{D} + \lambda_2 \frac{\delta \mathbf{D}}{\delta t}), \tag{22}$$

where λ_2 denotes the retardation time, λ_1 is the relaxation time and these material coefficients are such that $0 \leq \lambda_2 < \lambda_1$. The Oldroyd type fluids can be considered as Maxwell fluids with additional viscosity. This type of models (22) contain the previous (19) model and (2) as particular cases.

In order to better understand the theory of viscoelasticity it is useful to illustrate the typical behavior of viscoelastic materials by simple mechanical models, where a dashpot (piston moving inside a cylinder filled with liquid) represents a viscous (Newtonian) fluid and a spring stands for an elastic (Hookean) solid. These elements can be connected in series or in parallel and the analysis of the behavior of different viscoelastic materials can be done through their combinations representing various deformation-stress models [43, 81]. Figure 5 shows an elastic spring and a dashpot in series, representing the one-dimensional mechanical analogue to (19). Here, the speed of movement γ_V is an analogue of the rate of deformation, the coefficient of proportionality μ (for the viscous element) is an analogue of viscosity, γ_E can be treated as a relative deformation, G as the elastic modulus and the force $\boldsymbol{\tau}$ is an analogue of the extra stress $\boldsymbol{\tau}$ in (19). The ratio between the viscosity μ and elastic modulus G is hidden in the relaxation time parameter λ_1.

The combination of the Newtonian and the Maxwell models joined in parallel is shown in Fig. 6 which represents the mechanical analogue to the Oldroyd model (22).

Here the total viscosity μ is defined as $\mu = \mu_s + \mu_e$, where μ_s and μ_e are the solvent and the elastic (or polymeric) viscosity coefficients, respectively. Moreover,

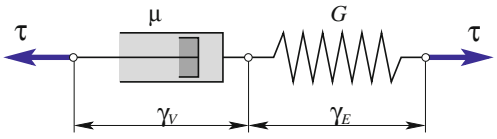

Fig. 5 Mechanical analogue of the Maxwell model

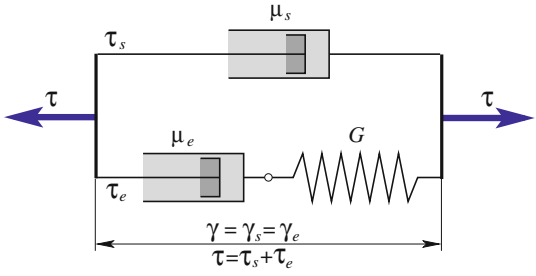

Fig. 6 Mechanical analogue of an Oldroyd-type model

parameters λ_1, λ_2 are defined by

$$\lambda_1 = \frac{\mu_e}{G}, \qquad \lambda_2 = \lambda_1 \frac{\mu_s}{\mu_s + \mu_e} \tag{23}$$

and, as stated above, they verify the inequality $0 \leq \lambda_2 < \lambda_1$ (assuming μ_e is not zero).

The total force $\boldsymbol{\tau}$ can be expressed as the sum of the Newtonian solvent contribution $\boldsymbol{\tau}_\mathbf{s}$ and its viscoelastic counterpart $\boldsymbol{\tau}_\mathbf{e}$. In a similar manner, the extra stress tensor $\boldsymbol{\tau}$ in Eq. (22) is decomposed into its Newtonian part $\boldsymbol{\tau}_s$ and its elastic part $\boldsymbol{\tau}_e$,

$$\boldsymbol{\tau} = \boldsymbol{\tau}_s + \boldsymbol{\tau}_e, \tag{24}$$

such that

$$\boldsymbol{\tau}_s = 2\mu_s \mathbf{D} \tag{25}$$

and $\boldsymbol{\tau}_e$ satisfies a constitutive equation of Maxwell type, namely

$$\boldsymbol{\tau}_e + \lambda_1 \frac{\delta \boldsymbol{\tau}_e}{\delta t} = 2\mu_e \mathbf{D}. \tag{26}$$

A one-parameter family of frame indifferent convected derivatives of a tensor $\boldsymbol{\tau}$ takes the general form

$$\left(\frac{\delta \boldsymbol{\tau}}{\delta t}\right)_a = \frac{D\boldsymbol{\tau}}{Dt} - \mathbf{W}\boldsymbol{\tau} + \boldsymbol{\tau}\mathbf{W} + a(\mathbf{D}\boldsymbol{\tau} + \boldsymbol{\tau}\mathbf{D}), \qquad a \in [-1, 1] \tag{27}$$

where $\mathbf{W}$ represents the anti-symmetric part of the velocity gradient. The particular value $a = -1$ corresponds to the upper-convected time derivative (20) (see e.g. [64]).

We now recall Eq. (26) for the elastic part of the extra stress tensor. It can be rewritten as

$$\frac{\delta \boldsymbol{\tau}_e}{\delta t} = \frac{2\mu_e}{\lambda_1}\mathbf{D} - \frac{1}{\lambda}\boldsymbol{\tau}_e \tag{28}$$

or, in terms of the classical material time derivative, as

$$\frac{D\boldsymbol{\tau}_e}{Dt} + \left(\frac{\delta \boldsymbol{\tau}_e}{\delta t} - \frac{D\boldsymbol{\tau}_e}{Dt}\right) = \frac{2\mu_e}{\lambda_1}\mathbf{D} - \frac{1}{\lambda_1}\boldsymbol{\tau}_e, \tag{29}$$

with the term in brackets representing a kind of "objective correction" of the material time derivative. Moving this term to the right-hand side and expanding

the remaining time derivative on the left, we get the following transport equation for $\boldsymbol{\tau}_e$

$$\frac{\partial \boldsymbol{\tau}_e}{\partial t} + (\mathbf{u} \cdot \nabla)\, \boldsymbol{\tau}_e = \frac{2\mu_e}{\lambda_1}\mathbf{D} - \frac{1}{\lambda_1}\boldsymbol{\tau}_e - \left(\frac{\delta \boldsymbol{\tau}_e}{\delta t} - \frac{D\boldsymbol{\tau}_e}{Dt}\right). \tag{30}$$

Using Eq. (27) with $a = -1$, corresponding to the upper-convected time derivative, transport equation (30) becomes

$$\frac{\partial \boldsymbol{\tau}_e}{\partial t} + (\mathbf{u} \cdot \nabla)\, \boldsymbol{\tau}_e = \frac{2\mu_e}{\lambda_1}\mathbf{D} - \frac{1}{\lambda_1}\boldsymbol{\tau}_e + (\mathbf{W}\boldsymbol{\tau}_e - \boldsymbol{\tau}_e\mathbf{W}) + (\mathbf{D}\boldsymbol{\tau}_e + \boldsymbol{\tau}_e\mathbf{D}). \tag{31}$$

This is the constitutive equation for the viscoelastic isothermal Oldroyd-B fluid.

The governing equations for the Oldroyd-B fluid are obtained by considering the basic principles of conservation of linear momentum and mass for isothermal incompressible flows, where the extra stress $\boldsymbol{\tau}$ is decomposed as in (24), the Newtonian part $\boldsymbol{\tau}_s$ being represented by (25) and the viscoelastic component $\boldsymbol{\tau}_e$ satisfying the constitutive equation (31).

Remark 1 An important non-dimensional parameter characterizing the viscoelastic effects in the flow is the *Weissenberg number* defined as $We = \frac{\lambda_1 U}{L}$, where U denotes a characteristic velocity and L is a characteristic length of the flow. In this case the Weissenberg number can be interpreted as the ratio between "memory" and advection time-scales. It relates the relaxation time to the time the fluid particle needs to pass the distance L while advected at speed U.

The Oldroyd-B model accounts for the viscoelasticity of blood but not for its shear-thinning behavior. However, replacing the constant viscosity μ in $\boldsymbol{\tau}_s$ by a shear dependent viscosity function $\mu(\dot{\gamma})$, i. e.

$$\boldsymbol{\tau}_s = 2\mu(\dot{\gamma})\mathbf{D}, \tag{32}$$

using, for instance one of the generalized Newtonian models listed in Table 3 with the corresponding parameters, we obtain a generalized Oldroyd-B (*GOB*) model that can be appropriate to describe blood flow behavior.

Other viscoelastic constitutive models of differential type, suitable to account for blood rheology have been proposed in the recent literature. The empirical five—constant generalized Oldroyd -B model studied in [132] belongs to this class. It is a shear-thinning Oldroyd-B model with the shear-dependent viscosity $\mu(\dot{\gamma})$ in (32) defined by

$$\mu(\dot{\gamma}) = \mu_\infty + (\mu_0 - \mu_\infty)\left[\frac{1 + \ln(1 + \Lambda\dot{\gamma})}{(1 + \Lambda\dot{\gamma})}\right]. \tag{33}$$

This viscosity function has been derived by fitting experimental data for steady capillary one-dimensional flows to determine the constants, $\mu_0 = 200\,\text{mPa s}$, $\mu_\infty = 6.5\,\text{mPa s}$ and $\Lambda = 11.14\,\text{s}$, and generalizing such curve fits to three dimensions.

The previous model captures the shear-thinning behavior of blood over a large range of shear rates but it has some limitations, since the relaxation times do not depend on the shear rate, which does not agree with experimental observations for blood. An appropriate model should consider blood as a viscoelastic fluid capable of instantaneous elastic response. The theory developed by Rajagopal and Srinivasa in [107] is particularly well suited to develop a model for blood. This framework needs the specification of how the body stores and dissipates energy, by introducing a precise Helmholtz potential associated with the body and a rate of dissipation function, respectively. However, not all viscoelastic fluids can be described within that earlier framework (see [107] for further details).

The model developed by Anand and Rajagopal [2], derived from the general thermodynamic framework stated in [107], includes relaxation times depending on the shear rate, gives good agreement with experimental data in steady Poiseuille and oscillatory flows and has proven to be successful in describing the response of blood. This model contains the Oldroyd-B model as a special sub-class and is particularly well suited to describe the instantaneous elastic response of blood, under physiological conditions. Numerical simulations in some idealized geometries to investigate the combined effects of flow inertia, viscosity and viscoelasticity, can be found in [19]. Anand et al. [1, 3] have also studied the problem of the formation and lysis of blood clots, as well as the problem of ATIII and protein C deficiency [4] within the context of the above model. See also numerical simulations in [117]. An improvement of this model can be found in [5].

The set of governing equations derived in [2], the so-called (*BModel*), are based on the principles of conservation of linear momentum and mass for an isothermal incompressible fluid, with the extra stress tensor decomposed as follows:

$$\mathbf{T} = -p\mathbf{I} + \eta\,\mathbf{B}_{\kappa_p(t)} + \mu_s\mathbf{D} \tag{34}$$

where η and μ_s are positive material parameters (μ_s is the Newtonian viscosity), $\mathbf{B}_{\kappa_p(t)}$ is the elastic stretch tensor and the subscript $\kappa_p(t)$ is used to emphasize that the stretch is expressed with respect to the natural (time dependent) configuration $\kappa_p(t)$.

The upper-convected time derivative of the elastic stretch tensor $\mathbf{B}_{\kappa_p(t)}$ can be written as

$$\delta\mathbf{B}_{\kappa_{p(t)}}/\delta t = \overset{\triangledown}{\mathbf{B}}_{\kappa_{p(t)}} =: -\frac{1}{\tau(\mathbf{B}_{\kappa_{p(t)}})}\left[\mathbf{B}_{\kappa_{p(t)}} - \lambda\mathbf{I}\right]. \tag{35}$$

Here $\tau = \tau(\mathbf{B}_{\kappa_{p(t)}})$ defined by

$$\frac{1}{\tau(\mathbf{B}_{\kappa_{p(t)}})} = 2K\left(\text{tr}(\mathbf{B}_{\kappa_{p(t)}}) - 3\lambda\right)^n. \tag{36}$$

(where K is a material parameter) has the dimension of time and plays a role similar to the relaxation time λ_1 in the classical Oldroyd-B (22) or Maxwell (19) models. The coefficient λ depends on the trace of the inverse of the tensor $\mathbf{B}_{\kappa_{p(t)}}$ according to

$$\lambda = \frac{3}{\mathrm{tr}\left(\mathbf{B}^{-1}_{\kappa_{p(t)}}\right)}. \tag{37}$$

Using the definition of the upper-convected time derivative (20), the left-hand side of (35) can be rewritten in a more conventional form in terms of the material time derivative:

$$\frac{D\mathbf{B}_{\kappa_{p(t)}}}{Dt} - \left[\mathbf{L}\mathbf{B}_{\kappa_{p(t)}} + \mathbf{B}_{\kappa_{p(t)}}\mathbf{L}^T\right] = -\frac{1}{\tau\left(\mathbf{B}_{\kappa_{p(t)}}\right)}\left[\mathbf{B}_{\kappa_{p(t)}} - \lambda\mathbf{I}\right] \tag{38}$$

Finally, expanding the material time derivative on the left-hand side we end up with

$$\frac{\partial\mathbf{B}_{\kappa_{p(t)}}}{\partial t} + (\mathbf{u}\cdot\nabla)\,\mathbf{B}_{\kappa_{p(t)}} = -\frac{1}{\tau}\left[\mathbf{B}_{\kappa_{p(t)}} - \lambda\mathbf{I}\right] + \left[\mathbf{L}\mathbf{B}_{\kappa_{p(t)}} + \mathbf{B}_{\kappa_{p(t)}}\mathbf{L}^T\right] \tag{39}$$

where the coefficients λ and τ are scalar functions of the tensor $\mathbf{B}_{\kappa_{p(t)}}$ and its invariants, according to (37) and (36), respectively.

It is interesting to remark that the constitutive equations (39) for the (*BModel*) and (31) for the classical Oldroyd-B (upper-convected Maxwell) model have a similar form.

Predictions of the coefficients for the proposed (*BModel*) in [2]

$$\mu_s = 0.01\,\mathrm{Pa\,s}; \quad \eta = 0.0227\,\mathrm{N/m^2}; \quad n = 0.7525; \quad K = 1.2056\,\mathrm{s}^{-1} \tag{40}$$

(with n positive to ensure the shear-thinning behavior) have been compared with the data for human blood [126].

More details related to the (*BModel*) and the notation used here can be found in [2, 107] and also in [16, 19] where its implementation has been performed and some numerical results have been obtained.

All models considered above can be solved for the variables velocity, pressure and shear stress, provided the viscosity function, flow parameters and appropriate boundary conditions are given.

With respect to boundary conditions for the Navier-Stokes and generalized Navier-Stokes equations, it is necessary to prescribe either the velocity or the surface traction force (Dirichlet or Neumann boundary conditions, respectively) at the inflow boundary. Usually, physiological data are not available and a fully developed Poiseuille velocity profile (or the Womersley solution, in the unsteady case) can be prescribed. This is an acceptable idealization of the inflow condition

in relatively long straight vessel segments. At the vessel wall, the no-slip condition, expressing that the velocity at the wall boundary is the wall velocity, is appropriate, if we consider rigid wall vessels. At the outflow boundary, a condition prescribing surface traction force can be applied.

The Oldroyd-B and generalized Oldroyd-B models are of mixed elliptic-hyperbolic type (or parabolic-hyperbolic, in the unsteady case). The extra stresses behave hyperbolic, which means that they are only determined by past time. For these models the boundary conditions are the same as for the Navier-Stokes and generalized Navier-Stokes equations, supplemented by the specification of all the stress components representing the fluid memory at the inlet boundary [64].

3 Numerical Simulations of Non-Newtonian Blood Flow Models

Several methods have been used in modeling and simulation of the Non-Newtonian effects in blood rheology, including analytical, stochastic and numerical methods (finite elements, finite differences, finite volumes, spectral collocation, particle methods). No single model can capture the complex blood characteristics and different models have been used to represent blood rheology. Since most of the Non-Newtonian characteristics derive from the behavior of RBCs in shear flows, in particular their concentration, distribution and mechanical properties, generalized Newtonian models, namely Carreau, Carreau-Yasuda and Cross (e.g. [8, 9, 16, 21, 22, 26, 49, 50, 52, 53, 61–63, 68, 74, 87, 106, 116]) are the most popular models found in literature. However, Casson (e.g. [57, 70, 83, 86, 87]) and shear-thinning viscoelastic models (e.g. [2–5, 18, 19, 58, 90, 132]) have also been largely used.

A comparative numerical study of three different test cases is presented to illustrate the influence of the shear-thinning and viscoelastic effects on the qualitative behavior of blood flow in rigid-walled medium sized idealized and realistic vessels, using some of the models described in the previous section.

Remark 2 Blood flow interacts mechanically with the vessel wall, resulting in pressure waves propagating in arteries, which deform under the action of blood pressure. In order to capture these phenomena, complex fluid-structure interaction (FSI) problems must be considered, coupling physiologically meaningful models for both the blood and the vessel wall. To simplify the presentation wall compliance is not considered in the test cases.

3.1 Numerical Simulations in Idealized Geometries

3.1.1 Stenosed Vessel

The first test case is a simple 2D non-symmetric (with respect to the bulk flow direction) channel with a local constriction, modeling a cosine-shape stenosed blood vessel, with 75% area reduction, represented in Fig. 7.

To account for the shear-thinning behavior of blood we choose the generalized Newtonian Carreau model defined in Sect. 2.3.2 (see Table 3)

$$\mu(\dot{\gamma}) = \mu_\infty + (\mu_0 - \mu_\infty)(1 + (\lambda\dot{\gamma})^2)^{(n-1)/2} \tag{41}$$

with material parameters

$$\mu_0 = 0.639\,\text{Pa s}; \quad \mu_\infty = 0.0045\,\text{Pa s}; \quad \lambda = 10.03\,\text{s}; \quad n = 0.35 \tag{42}$$

and, for the purpose of comparison, blood is also modeled as a Newtonian fluid with a constant viscosity $\mu = 0.0035\,\text{Pa s}$, corresponding an average experimental viscosity in the range $\dot{\gamma} \in [2, 1000]\,\text{s}^{-1}$. Blood density is $\rho = 1.06\,\text{g cm}^{-3}$, in both cases.

The experimental viscosity data used in this test case were obtained by M. Kameneva (Univ. Pittsburgh) for normal human blood at temperature $T = 23\,^\circ\text{C}$ and hematocrit $Ht = 40\%$ (see [108]. The main goal is to investigate the influence of inertia and shear-thinning effects on the qualitative behavior of blood flow in this idealized stenosed vessel.

For the numerical approximation of each one of the governing systems of PDEs, a backward Euler scheme is used for time discretization and, at each time step, a finite element space discretization of the velocity-pressure formulation (with P_2-P_1 elements) is implemented, using a splitting scheme with algebraic factorization (e.g. [103]). The computational domain is discretized into 2858 internal triangular elements and a boundary layer mesh consisting of 472 quadrilateral elements (Fig. 7). A fully developed Poiseuille parabolic velocity profile with flow rate $Q = 2.0\,\text{cm}^3/\text{s}$ is prescribed at the inlet and homogeneous Neumann conditions for the velocity components (zero normal stresses) are imposed at the outlet. The initial-boundary value problems are also endowed with an initial condition $\mathbf{u} = \mathbf{u}_0$, for $t = 0$, and with a no-slip boundary condition $\mathbf{u} = \mathbf{0}$ prescribed at the vessel wall.

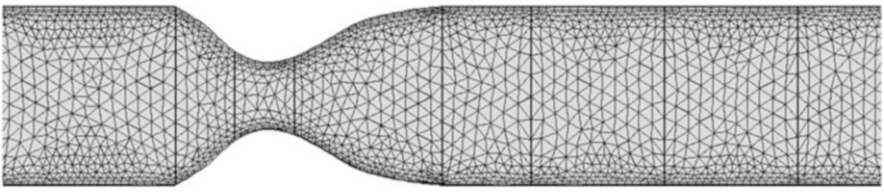

Fig. 7 Stenosed vessel: computational grid structure

Figures 8, 9 show a comparison between the velocity contours corresponding to the Newtonian (*NS*) and the Carreau models, with parameters introduced above, using the same color scale (units in m/s). As expected, in both figures we observe a similar behavior at the stenosis site, but the area reduction in the stenosed region leads to a significant local flow acceleration near the wall and the appearance of recirculation patterns corresponding to two regions of reversal flow, downstream the stenosis. In the two cases the flow structure is similar but the impact of the non-Newtonian effects in the flow separation behind the stenosis is non-negligible, with the velocity close to the wall developing a slower backflow in a larger region for the (*NS*) flow model than for the generalized Newtonian Carreau model. In the vessel's centreline the velocity profile is flatter for the Carreau flow, which corresponds to a reduction in the maximum velocity magnitude. As a result, the near wall flow is accelerated and thus the recirculation zones become shorter, compared to those for the (*NS*) flow.

This is a simple numerical study of the shear-thinning effects of the Carreau flow model compared to the inertial effects of the (*NS*) model. It could be completed by choosing different flow rates at the inflow boundary, other shear-thinning or viscoelastic shear-thinning models, as those derived in the previous Section, and the effect of the stenosis severity on the recirculation zone length downstream the stenosis. Moreover, hemodynamic flow indicators like the wall-shear stress (WSS) exerted on the wall, defined below (44), the time-averaged wall shear stress (TAWSS) or the oscillatory shear index (OSI) during a cardiac cycle, could also be investigated. This will be partially explored in the next test cases.

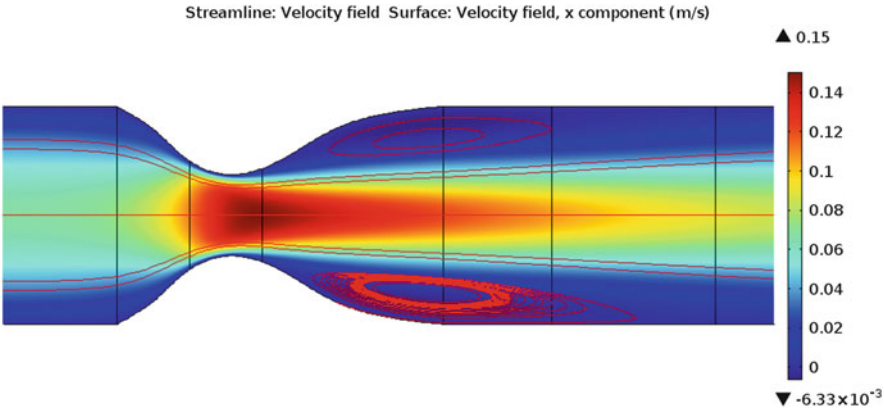

Fig. 8 Velocity magnitude contours and recirculation streamlines behind the stenosis for the Newtonian flow. A velocity legend is shown on the right

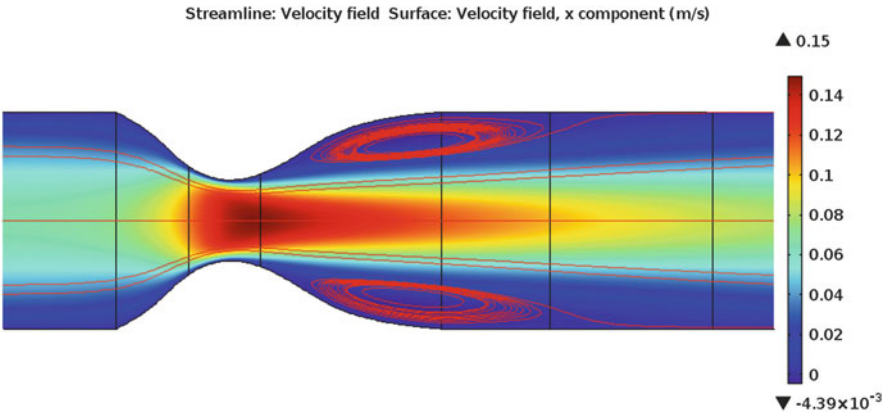

Fig. 9 Velocity magnitude contours and recirculation streamlines behind the stenosis for the generalized Newtonian flow. A velocity legend is shown on the right

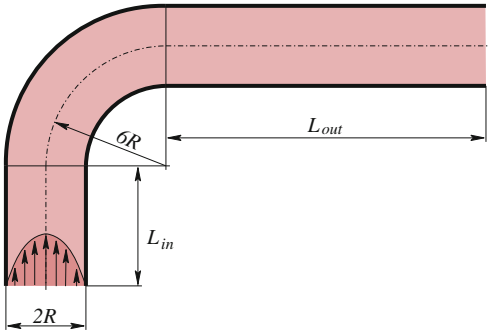

Fig. 10 Geometric representation of a curved vessel

3.1.2 Curved Vessel

Flows in curved vessels are significantly more complex than flows in straight vessels. For inertial Newtonian flows it is well known that a slight curvature of the vessel axis induces centrifugal forces on the fluid and, in addition to the primary initial flow, a secondary motion appears, sending fluid outward along the symmetry axis and returning along the upper and lower curved surfaces. This secondary motion is induced by a discrepancy between the cross-stream pressure gradient and the centrifugal forces developed at the curvature sites, and consists of a pair of symmetrical counter-rotating vortices that is superposed to the axial flow. This results in asymmetrical wall stresses with high shear and low pressure regions (see e.g. [6, 7, 13, 37]).

A 90° 3D curved vessel with circular cross-section (Fig. 10) has been chosen as a second test case, to study the shear-thinning and viscoelastic effects in the presence of high streamline curvature and non-negligible secondary flows (see [19]).

Numerical simulations have been performed to compare the predictions of the above described shear-thinning viscoelastic fluid model for blood flow (39), further denoted as (*BModel*), with those of the classical Newtonian (*NS*) model and a generalized Oldroyd-B (*GOB*) model. The material parameters used for the (*BModel*) are those listed in (40). The (*GOB*) model used here is obtained from the Oldroyd-B model (31) replacing the total (constant) viscosity by the shear dependent viscosity given by the modified Cross function defined in Sect. 2.3.2

$$\mu(\dot{\gamma}) = \mu_\infty + (\mu_0 - \mu_\infty)\frac{1}{(1 + (\lambda\dot{\gamma})^m)^a} \tag{43}$$

The asymptotic viscosities μ_0 and μ_∞ at low and high shear rates, have been adjusted to fit the *bModel*'s parameters, namely $\mu_0 = 0.0736\,\text{Pa s}$ and $\mu_\infty = 0.005\,\text{Pa s}$ and the parameters λ, m and a, estimated by curve fitting of experimental data, have been taken from [17] (see also [71]).

The numerical method used to solve the governing equations is based on a spatial finite-volume discretization on structured grids and an explicit Runge-Kutta time-stepping scheme, namely a robust modified Runge-Kutta four-stage method [60]. The computational mesh is structured and consists of hexahedral primary control volumes. To evaluate the viscous numerical fluxes also dual finite volumes with octahedral shape and centered around the primary cell faces are used.

The space discretization is based on a simple central finite-volume discretization on a structured wall-fitted mesh with hexahedral cells and non-uniform axial cell spacing. A multiblock grid topology was used to avoid high distortion of cells. The viscous fluxes are also discretized in a finite-volume style over a diamond-shaped cells adjoint to primary control volumes faces.

A pressure stabilization technique has been used in the present simulations (see e.g. [130]) to avoid numerical oscillations in the pressure, which are mainly due to the presence of strong gradients. Moreover, since the Reynolds number used in the simulations was quite low (of the order of 10^2), no additional stabilization was needed for the flow variables. This approach has been adopted in earlier papers. For further details see e.g. [16–19] and the references therein.

A parabolic velocity profile with flow rate $Q = 2.0\,\text{cm}^3/\text{s}$, prescribed at the inlet of the curved vessel has been considered for the simulations of the *bModel* and the *GOB* and *NS* models. This flow rate is sufficiently high to capture the secondary flows pattern (see Fig. 12). Homogeneous Neumann conditions for the velocity components were imposed at the outlet and no-slip conditions were prescribed at the vessel wall. Pressure was fixed at the outlet and extrapolated at the other boundaries. Moreover, in the case of the *bModel*, homogeneous Neumann boundary conditions were prescribed at all boundaries for the components of tensor $\mathbf{B}_{\kappa_p(t)}$. As an alternative, some simulations have been performed using a Dirichlet type boundary condition $\mathbf{B}_{\kappa_p(t)} = \mathbf{1}$ prescribed at the inlet, but no significant impact on the solution has been found.

One of the important features of the flow predicted by the *bModel* is related to the axial velocity profile. This can clearly be observed in Fig. 11 showing, for the three models *NS*, *GOB* and *bModel*, plots of the axial velocity profiles in three different

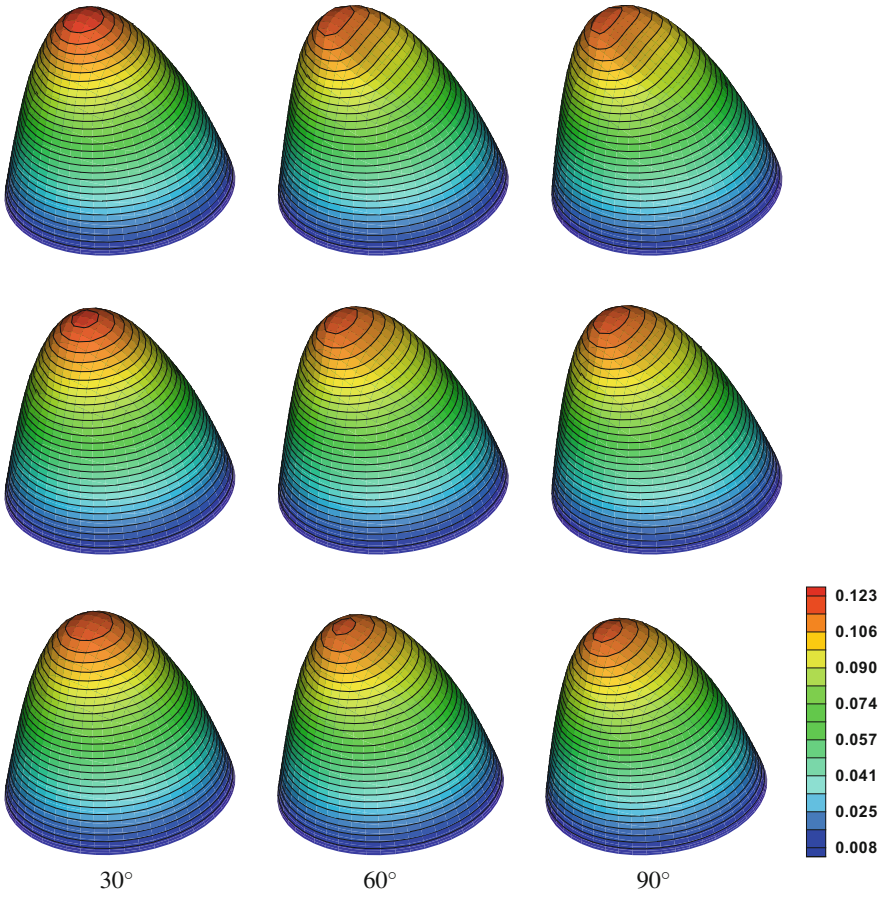

Fig. 11 Axial velocity profiles for *NS* flows (top row), *GOB* flows (middle row) and *bModel* flows (bottom row) in three different cross-sections at the bended part of the curved vessel (30°, 60°, 90°)

cross-sections of the curved vessel, placed at 30°, 60° and 90°. In the case of the *bModel* and *GOB* model flatter axial velocity profiles are obtained when compared to the *NS* model. As in the case of the flow in the stenosed vessel, this effect can be attributed to the shear-thinning behavior predicted by the first two models where the low shear rates around the centerline of the vessel lead to a local increase of the apparent viscosity. Based on these simulations, we can conclude that the shear-thinning effect is dominant when compared to the viscoelastic one. However, further numerical experiments could be performed to confirm this assumption.

Curvature effects are observed in the contours of the axial velocity, which are shifted away from the central axis as the curvature of the vessel increases from 30° to 90° (see Fig. 12 and, more clearly, Fig. 13). Secondary flow streamlines have a similar qualitative behavior for the three models *NS*, *GOB* and *bModel*, as shown in

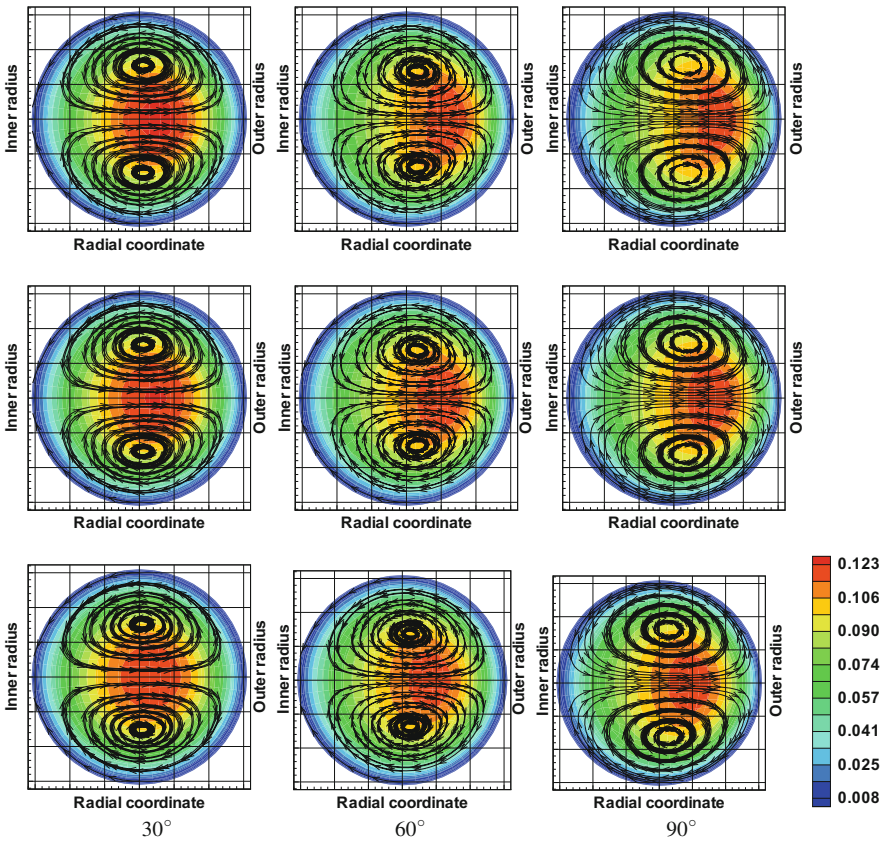

Fig. 12 Axial velocity magnitude contours and secondary flow streamlines for the *NS* (top row), *GOB* (middle row) and the *bModel* flows (bottom row) in three different cross-sections at the bended part of the curved vessel (30°, 60°, 90°)

Fig. 12. Further differences are visible while comparing the axial and radial velocity contours shown in Figs. 13 and 14. From Fig. 14 we realize that the magnitude of the secondary flow velocities is clearly lower for the models *GOB* and *bModel* than for the *NS* model, due to the shear-thinning behavior captured by the first two models for which lower shear rates lead to a higher apparent viscosity.

Figures 15 and 16 show the relative axial velocity differences (normalized by the characteristic velocity U) between the *bModel* and the classical *NS* model (Fig. 15, left and Fig. 16, top row) and between the two shear-thinning viscoelastic models *bModel* and *GOB* (Fig. 15, right and Fig. 16, bottom row). The color scale (in physical units m/s) is used to emphasize the set of flow regions varying from those where differences of solutions can be neglected (in black) to regions of the highest difference in the flow regime (in red or dark blue). The differences on the axial velocity between the *bModel* and the Newtonian model along the curved vessel

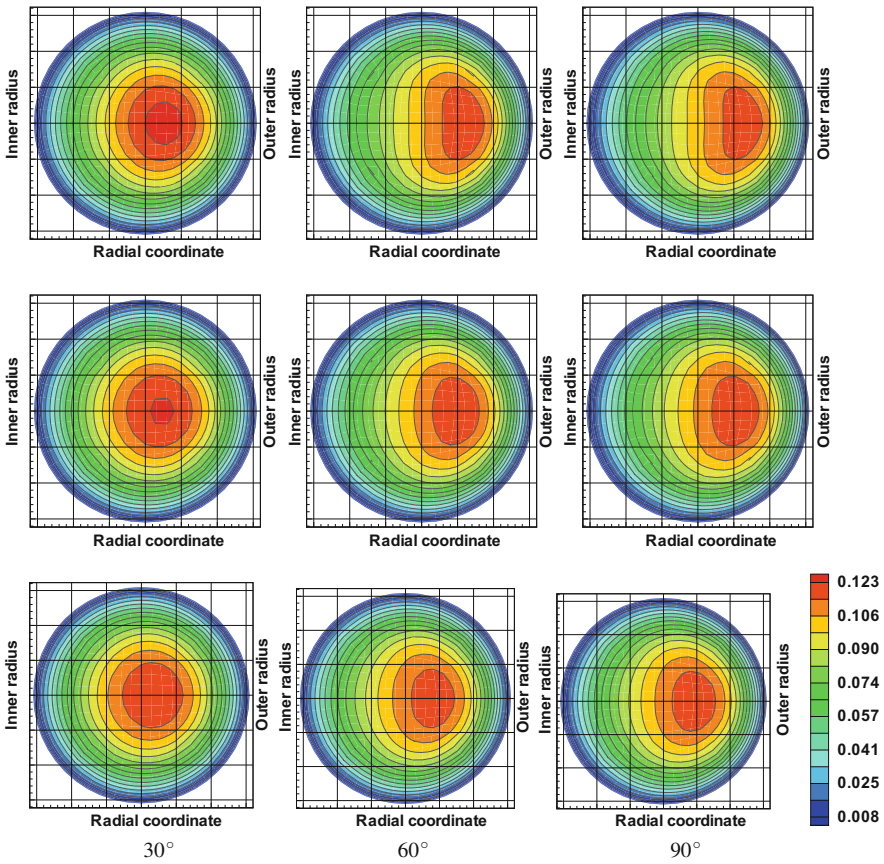

Fig. 13 Axial velocity magnitude contours for the *NS* (top row), *GOB* (middle row) and the *bModel* flows (bottom row) in three different cross-sections at the bended part of the curved vessel (30°, 60°, 90°)

(Fig. 15, left) show the expected slow-down of the core flow (caused by the shear-thinning behavior) in the straight inlet part of the vessel. This is compensated by a faster near-wall flow. As soon as the flow reaches the bended part of the curved vessel, the slow core of the flow is pushed towards the outer wall (see top row in Fig. 16 for a more detailed view), while close to the inner radius of the bend, the flow accelerates. A similar (although weaker) tendency of the flow behavior can also be seen for the difference between the *bModel* and *GOB* models (Fig. 15, right and Fig. 16, low row). This is mainly due to the fact that both models have a shear-thinning viscosity. In the *bModel* shear-thinning effects seem to be slightly more pronounced than in the *GOB* model.

To summarize, we conclude that results obtained with both *bModel* and *GOB* blood flow models are very similar, when compared to those obtained with the

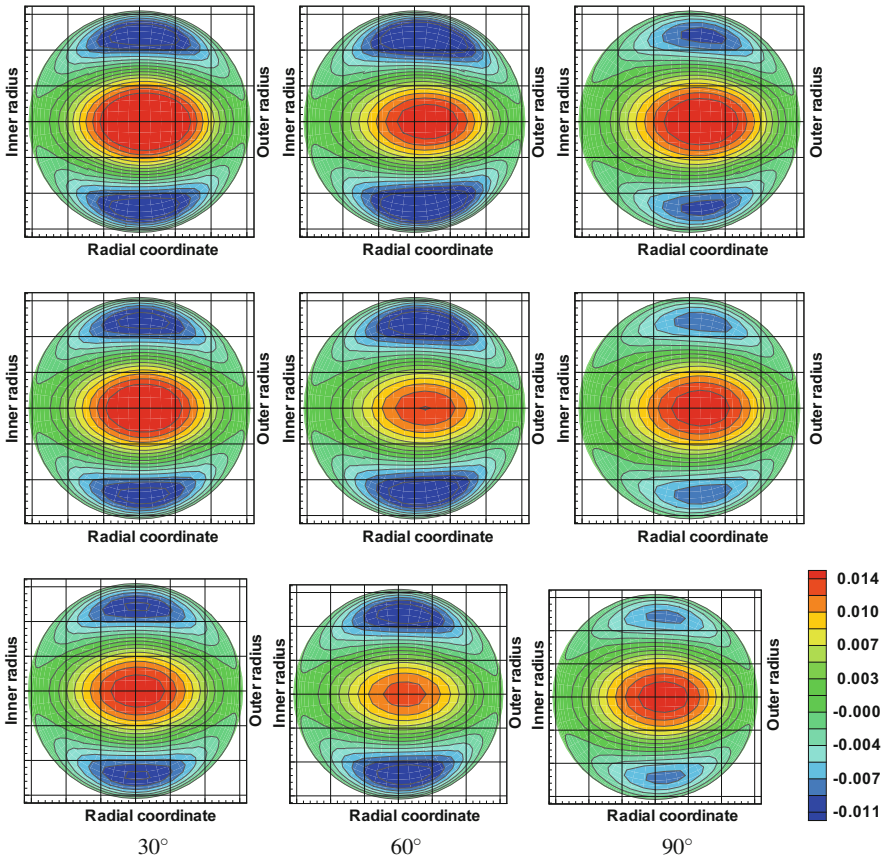

Fig. 14 Radial velocity magnitude contours for the *NS* (top row), *GOB* (middle row) and the *bModel* flows (bottom row) in three different cross-sections at the bended part of the curved vessel (30°, 60°, 90°)

NS model, showing in particular that the more complex *bModel* has been properly implemented and that the shear-thinning and viscoelastic rheological characteristics are dominant with respect to inertia. Future numerical simulations in curved vessels with different curvatures can provide a deeper insight into this investigation.

3.2 Numerical Simulations in a Realistic Geometry: Stenosed Carotid Bifurcation

Now we consider an anatomically 3D realistic model of a diseased human carotid bifurcation, smoothly reconstructed from an MRI medical image, as shown in

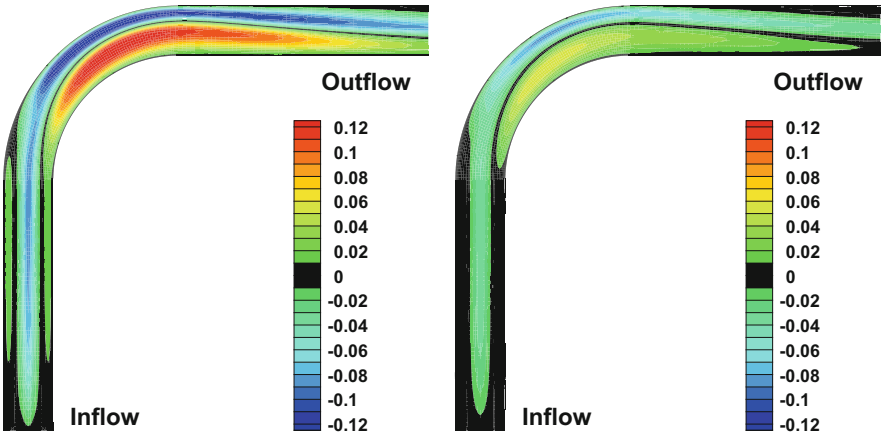

Fig. 15 Relative difference of the axial velocity along the curved vessel $(u_{bModel} - u_{NS})/U$ (left) and $(u_{bNOB} - u_{GOB})/U$ (right)

Fig. 17. The common carotid artery bifurcates into the internal and external carotid arteries that supply blood into the brain and the face, respectively. A stenosis of about 75% has been generated in the internal carotid artery (ICA), near the bifurcation region, where narrowing or constrictions of the arterial inner surface, caused by atherosclerosis usually occur and are responsible for about 10% of ischemic strokes. The accumulation of plaques on the arterial wall is a progressive disease accelerated by local irregular flow fields such as separation and flow-reversal zones, which already occur at milder degrees of stenosis. It is well established that once a mild stenosis is formed in the artery, altered blood flow and stress distribution in the arterial wall contribute to further progression of the disease.The present study can be regarded as a follow-up investigation of the influence of hemodynamic factors on atherosclerosis development, after the disease has been recognized.

The main goal is to investigate inertial and shear-thinning effects in unsteady simulations using the time-dependent incompressible Newtonian (*NS*) and the generalized Newtonian Carreau models defined in Sect. 2.3.2, see also (41). The shear-thinning viscosity parameters used in this study are the physiological values previously used for the Carreau model in the first test case (42), Sect. 3.1. For the Newtonian model we also impose a constant viscosity $\mu = 0.0035$ Pa s, and blood density is $\rho = 1.06\,\mathrm{g\,cm^{-3}}$, in both cases. A fully developed laminar velocity profile with flow rate $Q = 5.5\,\mathrm{cm^3/s}$ is imposed at the inlet of the central carotid artery (main branch before bifurcation). Since the inflow diameter is 0.62 cm, this mean physiologic flow rate $Q = 5.5\,\mathrm{cm^3/s}$ results in a Reynolds number $Re = 300$ in the Newtonian case. The diameters of the outflow sections of the internal and external carotid arteries are equal to 0.25 cm and 0.22 cm, respectively. The total length of the domain, from upstream to downstream is approximately 5.4 cm. No-slip boundary conditions are imposed at the vessel wall.

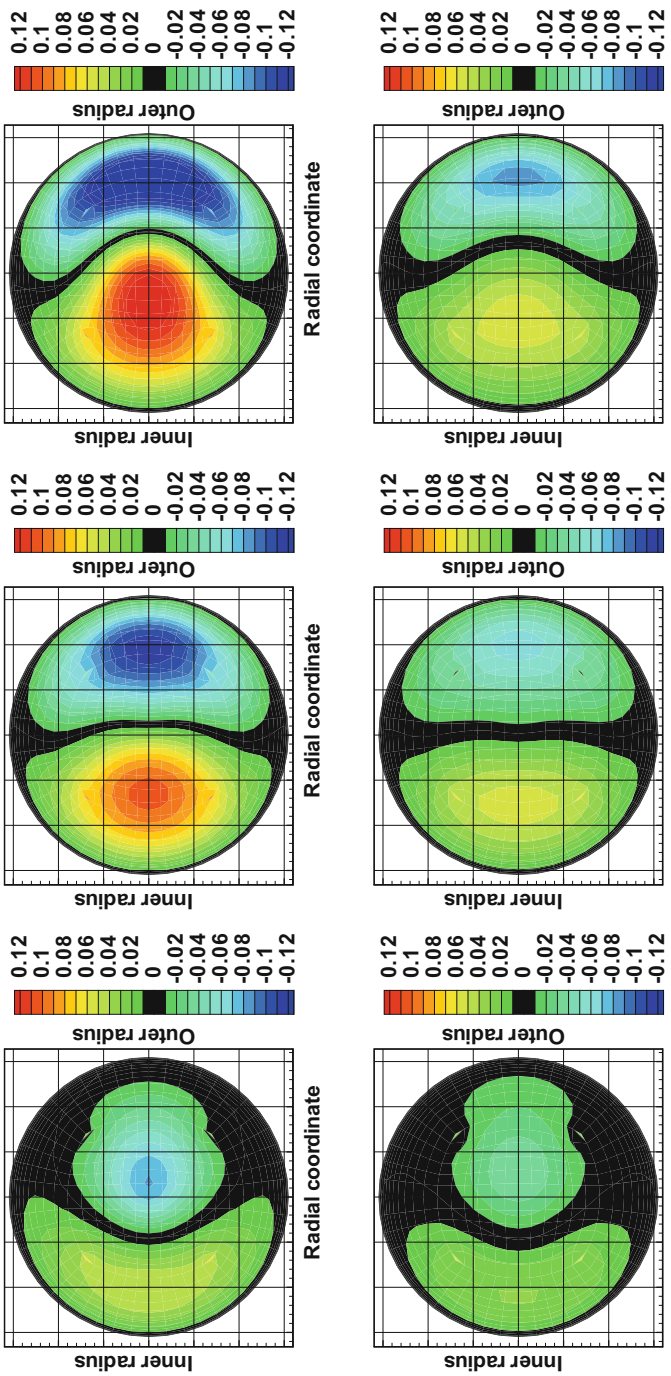

Fig. 16 Relative differences between the axial velocity magnitude contours $(u_{bModel} - u_{NS})/U$ (top row) and $(u_{bModel} - u_{GOB})/U$ (bottom row) in three different cross-sections at the bended part of the curved vessel (30°, 60°, 90°)

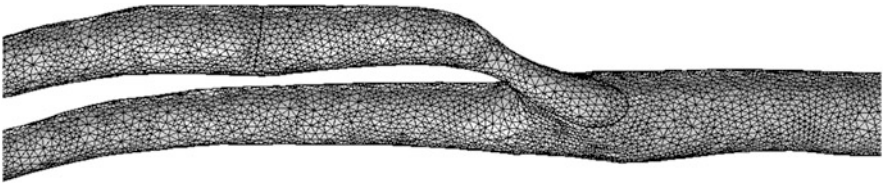

Fig. 17 Computational mesh used for the blood flow simulations in a stenosed carotid artery bifurcation

The conditions applied at the outlets are usually imposed in order to guarantee the well-posedness of the differential problems, for sufficiently smooth and small data. As in the previous test cases, we impose the "standard" homogeneous Neumann conditions at the outlets. However, these conditions are unphysical for the case of a human vessel, since they neglect completely the presence of the remaining part of the circulatory system, which is usually not implemented using a 3D model due to the limited capacity of current computers. Moreover, only averaged data (mean velocity and mean pressure values) are available at the artificial boundaries and alternative boundary conditions need to be used, reflecting the physics of the given problem. A possible strategy consists in coupling the 3D Navier-Stokes (or the generalized Navier-Stokes) equations with reduced 1D (distributed parameter) or 0D (lumped parameter) approximations of the full equations that, in a simplified way, can represent the remaining part of the circulatory system and act as absorbing boundary conditions. The coupling of these heterogeneous models, using appropriate transmission conditions and efficient techniques for their numerical computation, usually called *geometrical multiscale* approach, represents a decreased level of accuracy which is compensated by its lower computational cost. This issue has been addressed by several authors and is still nowadays a matter of active research (see e.g. [104] for a recent overview referring to the original works on the subject)

A finite element approach has been adopted for the numerical solution of the governing equations associated to both models. The patient-specific geometry is discretized with 327,896 tetrahedral elements. A backward Euler scheme is used for time discretization and, at each time step (0.5×10^{-3} s), a velocity-pressure splitting scheme with algebraic factorization is implemented to discretize in space (see, e.g. [103]). Lagrange low order $P_1 - P_1$ elements have been adopted and this requires stabilization techniques like the Streamline upwind/Petrov Galerkin method (SUPG-method) in order to avoid oscillations in the numerical solutions [59]. The SUPG-method yields a substantial increase in accuracy because stabilizing artificial diffusivity is added only in the direction of the streamlines and crosswind diffusion effects are avoided.

An important commonly adopted flow indicator is the wall shear stress (WSS). Knowing the velocity and pressure fields it is possible to obtain stresses, in particular WSS which represents the tangential component of the surface force at the vessel

wall, acting against the fluid flow.

$$WSS := -(\boldsymbol{\tau} \cdot \mathbf{n}) \cdot \mathbf{t}. \tag{44}$$

Here $\mathbf{n}$ is the local wall-normal unit vector (pointing towards the fluid domain) and $\mathbf{t}$ is the corresponding unit tangential vector.

WSS may cause alterations in the endothelium and has a great influence in many inflammatory diseases, including atherosclerosis, the development of aneurysms and clotting.

Hemodynamics in the stenosed carotid bifurcation was assessed in terms of the streamlines, magnitude of the velocity vector field and WSS distribution downstream the stenosis.

The difference between the solutions obtained using the *NS* model and generalized Newtonian Carreau model can be observed in Fig. 18 representing the

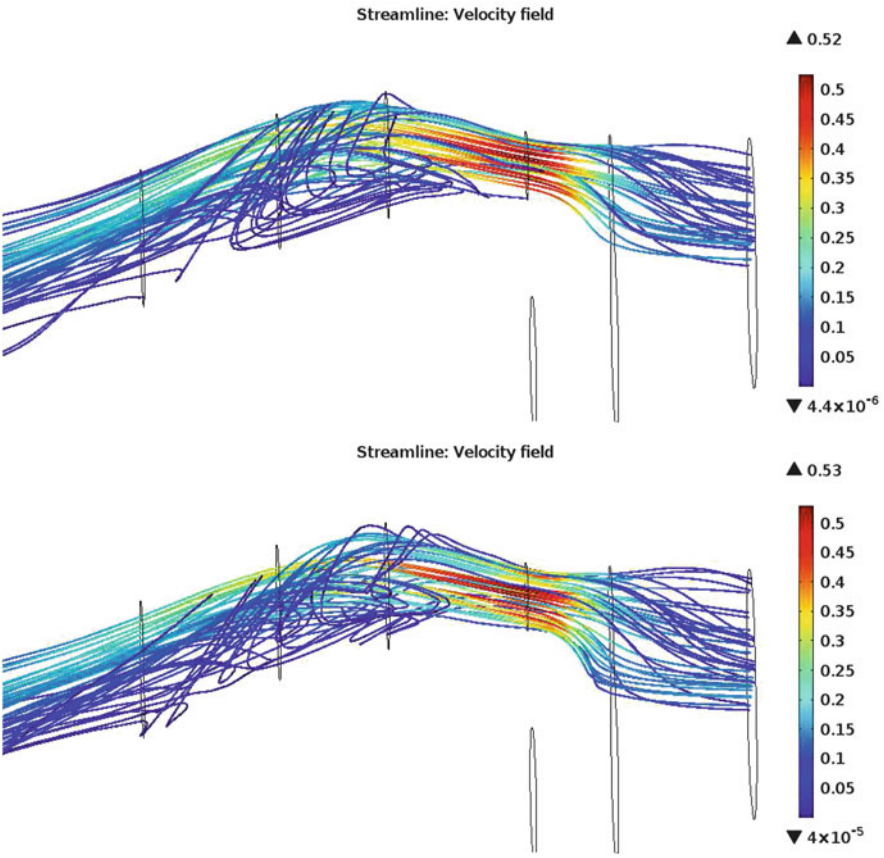

Fig. 18 Streamlines in the recirculation area downstream the stenosis in the ICA branch: for the *NS* flow (top); for the generalized Newtonian flow (bottom)

streamlines behind the stenosed region of ICA for both models. As expected, the flow behavior behind the stenosis site is quite similar, with the presence of reversal flow streamlines due to the local flow acceleration. However, the shear-thinning effects are quite visible, since the density of recirculating streamlines for the Newtonian flow is higher than for the non-Newtonian one, due to the local increase of the apparent viscosity at low shear rates, which become closer to μ_0. This also results in a larger recirculation region for the Newtonian flow, as seen in Fig. 19, when compared to Fig. 20, where the recirculation zones are marked in grey color.

Comparing the wall shear stress distribution, depicted in Figs. 21 and 22 we conclude that the higher WSS values are located in the stenosed region predicted by

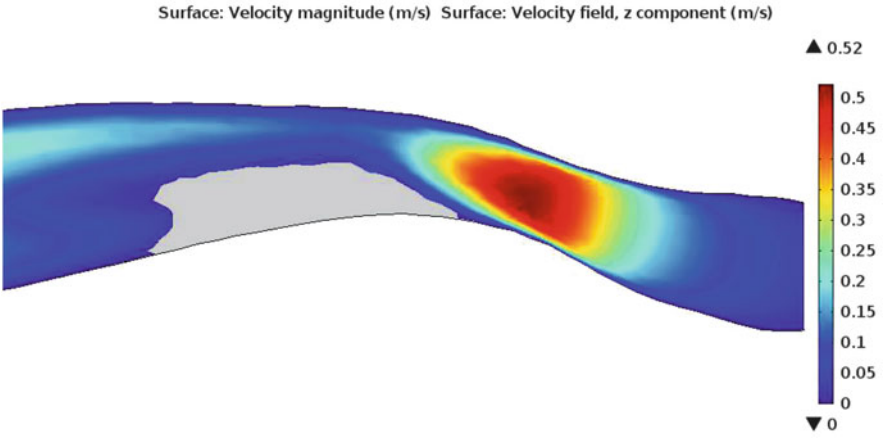

Fig. 19 Axial velocity magnitude contours and recirculation area downstream the stenosis in the ICA branch for the *NS* flow

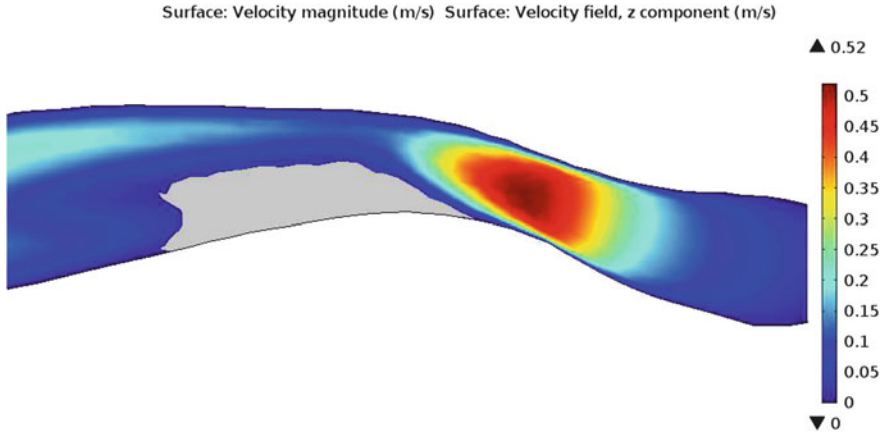

Fig. 20 Axial velocity magnitude contours and recirculation area downstream the stenosis in the ICA branch for the generalized Newtonian flow

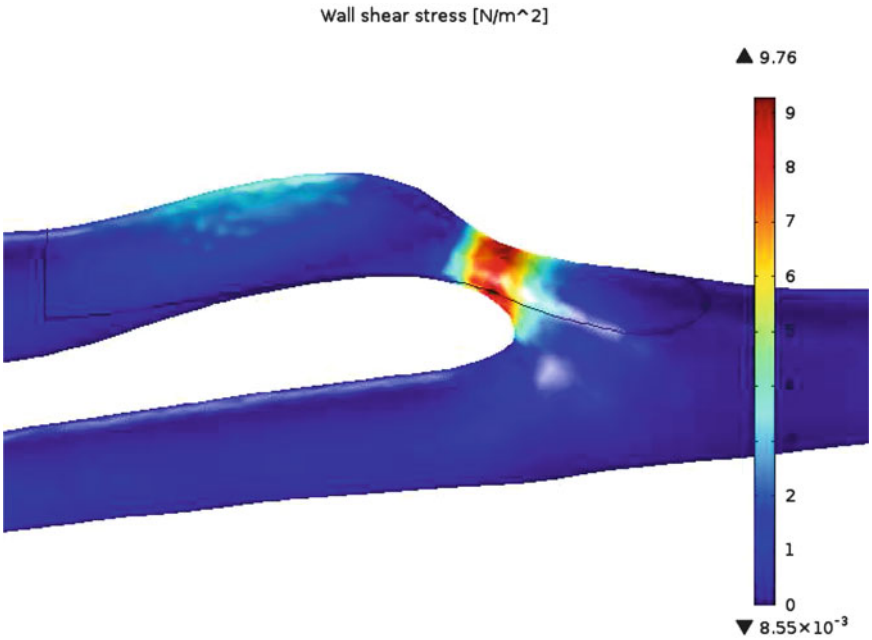

Fig. 21 Contours of the wall shear stress (WSS) distribution for the *NS* flow

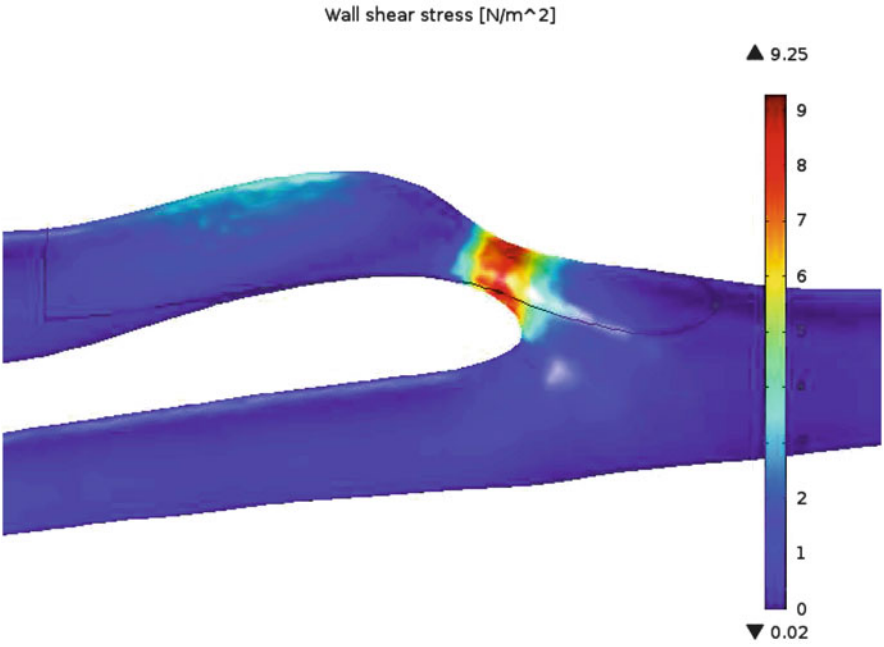

Fig. 22 Contours of the wall shear stress (WSS) distribution for the generalized Newtonian flow

the generalized Newtonian model. Also in the curved part of the stenosed branch, WSS seems to be slightly higher in the shear-thinning case. The reason for this is likely related to the non-uniform viscosity distribution along the vessel, leading to important discrepancies between Newtonian and generalized Newtonian model predictions. Therefore, it is of major importance to understand the influence of the viscosity distribution in complex flow situations.

Acknowledgements This research was partially supported by FCT—Fundação para a Ciência e a Tecnologia through the PHYSIOMATH project—"Mathematical and Computational Modeling of Human Physiology" (EXCL/MAT-NAN/0114/2012) and the Project UID/Multi/04621/2013 of the CEMAT—Center for Computational and Stochastic Mathematics, Instituto Superior Técnico, University of Lisbon.

References

1. Anand, M., Rajagopal, K., Rajagopal, K.R.: A model incorporating some of the mechanical and biochemical factors underlying clot formation and dissolution in flowing blood. Comput. Math. Methods Med. **5**(3–4), 183–218 (2003)
2. Anand, M., Rajagopal, K.R.: A shear-thinning viscoelastic fluid model for describing the flow of blood. Int. J. Cardiovasc. Med. Sci. **4**(2), 59–68 (2004)
3. Anand, M., Rajagopal, K., Rajagopal, K.R.: A model for the formation and lysis of blood clots. Pathophysiol. Haemost. Thromb. **34**, 109–120 (2005)
4. Anand, M., Rajagopal, K., Rajagopal, K.R.: A model for the formation, growth, and lysis of clots in quiescent plasma. A comparison between the effects of antithrombin III deficiency and protein C deficiency. J. Theor. Biol. **253**(4), 725–738 (2008)
5. Anand, M., Kwack, J., Masud, A.: A new Oldroyd-B model for blood in complex geometries. Int. J. Eng. Sci. **72**, 78–88 (2013)
6. Arada, N., Pires, M., Sequeira, A.: Numerical simulations of shear-thinning Oldroyd-B fluids in curved pipes. IASME Trans. **6**(2), 948–959 (2005)
7. Arada, N., Pires, M., Sequeira, A.: Viscosity effects on flows of generalized Newtonian fluids through curved pipes. Comput. Math. Appl. **53**, 625–646 (2007)
8. Artoli, A.M., Sequeira, A.: Mesoscopic simulations of unsteady shear-thinning flows. In: Computational Science - ICCS, pp. 78–85 (2006)
9. Artoli, A.M., Sequeira, A., Silva-Herdade, A.S., Saldanha, C.: Leokocytes rolling and recruitment by endothelial cells: hemorheological experiments and numerical simulations. J. Biomech. **40**, 3493–3502 (2007)
10. Astarita, G., Marrucci, G.: Principles of Non-Newtonian Fluid Mechanics. McGraw Hill, New York (1974)
11. Barnes, H.A.: Thixotropy - a review. J. Non-Newtonian Fluid Mech. **70**, 1–33 (1997)
12. Bauer, W.H., Collins, E.A.: Thixotropy and dilatancy. In: Eirich, F.R. (ed.) Rheology, Theory and Applications, vol. 4. Academic, New York (1967)
13. Berger, A.A., Talbot, L., Yao, L.-S.: Flow in curved pipes. Annu. Rev. Fluid Mech. **15**, 461–512 (1983)
14. Bingham, E.C.: An investigation of the laws of plastic flow. U.S. Bur. Stand. Bull. **13**, 309–353 (1916)
15. Bishop, J.J., Popel, A.S., Intaglietta, M., Johnson, P.C.: Relashionship between erythrocyte aggregate size and flow rate in skeletal muscle venules. Am. J. Physiol. **286**, H113–H120 (2004)

16. Bodnár, T., Sequeira, A.: Numerical simulation of the coagulation dynamics of blood. Comput. Math. Methods Med. **9**(2), 83–104 (2008)
17. Bodnár, T., Sequeira, A.: Numerical study of the significance of the non-Newtonian nature of blood in steady flow through a stenosed vessel. In: Rannacher, R., Sequeira, A. (eds.) Advances in Mathematical Fluid Mechanics, pp. 83–104. Springer, Berlin (2010)
18. Bodnár, T., Sequeira, A., Pirkl, L.: Numerical simulations of blood flow in a stenosed vessel under different flow rates using a generalized Oldroyd-B Model. Numerical Analysis and Applied Mathematics, vol. 2, pp. 645–648. American Institute of Physics, New York (2009)
19. Bodnár, T., Rajagopal, K.R., Sequeira, A.: Simulation of the three-dimensional flow of blood using a shear-thinning viscoelastic fluid model. Math. Model. Nat. Phenom. **6**(5), 1–24 (2011)
20. Bodnár, T., Fasano, A., Sequeira, A.: Mathematical Models for Blood Coagulation. In: Bodnár, T., Galdi, G.P., Nečasová, S. (eds.) Fluid-Structure Interaction and Biomedical Applications. Advances in Mathematical Fluid Mechanics, Chap. 7, pp. 483–569, Birkhäuser, Basel (2014)
21. Box, F.M.A., van der Geest, R.J., Rutten, M.C.M., Reiber, J.H.C.: The Influence of flow, vessel diameter, and Non-Newtonian blood viscosity on the wall shear stress in a carotid bifurcation model for unsteady flow. Investig. Radiol. **40**(5), 277–294 (2005)
22. Boyd, J., Buick, J.M., Green, S.: Comparison of Newtonian and Non-Newtonian oscillatory flows using the Lattice Boltzmann method. In: World Congress on Medical Physics and Biomedical Engineering, IFMBE Proceedings, vol. 14, pp. 3395–3399 (2007)
23. Čanić, S., Hartley, C.J., Rosenstrauch, D., Tambača, J., Guidoboni, G., Mikelić, A.: Blood flow in compliant arteries: an effective viscoelastic reduced model, numerics and experimental validation. Ann. Biomed. Eng. **34**(4), 575–592 (2006)
24. Caro, C.G., Pedley, T.J., Schroter, R.C., Seed, W.A., Parker, R.H.: The Mechanics of the Circulation, 2nd edn. Oxford University Press, Oxford (2012)
25. Charm, S.E., Kurland, G.S.: Blood Flow and Microcirculation. Wiley, New York (1974)
26. Chen, J., Lu, X.-Y., Wang, W.: Non-Newtonian effects of blood flow on hemodynamics in distal vascular graft anastomoses. J. Biomech. **39**, 1983–1995 (2006)
27. Chien, S.: Red cell deformability and its relevance to blood flow. Ann. Rev. Physiol. **49**, 177–192 (1987)
28. Chien, S., Usami, S., Dellenback, R.J., Gregersen, M.I.: Shear dependence of effective cell volume as a determinant of blood viscosity. Science **168**, 977–979 (1970)
29. Chien, S., Usami, S., Dellenback, R.J., Gregersen, M.I.: Shear-dependent deformation of erythrocytes in rheology of human blood. Am. J. Physiol. **219**, 136–142 (1970)
30. Chien, S., King, R.G., Skalak, R., Usami, S., Copley, A.L.: Viscoelastic properties of human blood and red cell suspensions. Biorheology **12**, 341–346 (1975)
31. Cho, Y.I., Kensey, K.R.: Effects of the Non-Newtonian viscosity of blood on flows in a diseased arterial vessel. Part I: steady flows. Biorheology **28**, 241–262 (1991)
32. Dintenfass, L.: Blood Microrheology - Viscosity Factors in Blood Flow, Ischaemia and Thrombosis. Butterworth, London (1971)
33. Dintenfass, L.: Blood Viscosity, Hyperviscosity and Hyperviscosaemia. MTP Press Ltd, Lancaster (1985)
34. Dong, C., Lei, X.X.: Biomechanics of cell rolling: shear flow, cell-surface adhesion and cell deformability. J. Biomech. **33**(1), 35–43 (2000)
35. Dupin, M.M., Halliday, I., Care, C.M., Alboul, L., Munn, L.L.: Modeling the flow of dense suspensions of deformable particles in three dimensions. Phys. Rev. E **75**, 066707 (2007)
36. Evans, E.A., Hochmuth, R.M.: Membrane viscoelasticity. Biophys. J. **16**(1), 1–11 (1976)
37. Fan, Y., Tanner, R.I., Phan-Thien, N.: Fully developed viscous and viscoelastic flows in curved pipes. J. Fluid Mech. **440**, 327–357 (2001)
38. Fasano, A., Sequeira, A.: Hemomath. The Mathematics of Blood. MS&A - Modeling, Simulation and Applications Series, vol. 18. Springer, Cham (2017). ISBN: 978-3-319-60512-8
39. Fasano, A., Santos, R., Sequeira, A.: Blood coagulation: a puzzle for biologists, a maze for mathematicians. In: Ambrosi, D., Quarteroni, A., Rozza, G. (eds.) Modelling Physiological Flows, Chap. 3, pp. 44–77. Springer Italia, Milano (2011). https://doi.org/10.1007/978-88-470-1935-53

40. Feher, J.J.: Quantitative Human Physiology: An Introduction. Elsevier, Academic, Amsterdam, New York (2012)
41. Fåhraeus, R.: The suspension stability of blood. Physiol. Rer. **9**, 241–274 (1929)
42. Fåhraeus, R., Lindqvist, T.: The viscosity of blood in narrow capillary tubes. Am. J. Physiol. **96**, 362–368 (1931)
43. Ferry, J.D.: Viscoelastic Properties of Polymers. Wiley, New York (1980)
44. Formaggia, L., Perktold, K., Quarteroni, A.: Basic mathematical models and motivations. In: Formaggia, L., Quarteroni, A., Veneziani, A. (eds.) Cardiovascular Mathematics. Modeling and Simulation of the Circulatory System, vol. 1, pp. 46–75. Springer, Berlin (2009)
45. Fung, Y.C.: Biomechanics: Circulation. Springer, New York (1997)
46. Gabe, I.T., Gault, J.H., Ross, J., Mason, D.T., Mills, C.J., Schillingford, J.P., Braunwald, E.: Measurement of instantaneous blood flow velocity and pressure in conscious man with a catheter-tip velocity probe. Circulation **40**, 603–614 (1969)
47. Galdi, G.P.: An Introduction to the Mathematical Theory of the Navier-Stokes Equations: Linearised Steady Problems. Springer Tracts in Natural Phylosophy, 2nd Corrected edn., vol. 38. Springer, Berlin (1998)
48. Galdi, G.P.: An Introduction to the Mathematical Theory of the Navier-Stokes Equations: Nonlinear Steady Problems. Springer Tracts in Natural Phylosophy, 2nd Corrected edn., vol. 39, Springer, Berlin (1998)
49. Gambaruto, A.M., Janela, J., Moura, A., Sequeira, A.: Sensitivity of hemodynamics in a patient specific cerebral aneurysm to vascular geometry and blood rheology. Math. Biosci. Eng. **8**(2), 409–423 (2011)
50. Gambaruto, A., Janela, J., Moura, A., Sequeira, A.: Shear-thinning effects of hemodynamics in patient-specific cerebral aneurysms. Math. Biosci. Eng. **10**(3), 649–665 (2013)
51. Gaspar-Rosas, A., Thurston, G.B.: Erythrocyte aggregate rheology by transmitted and reflected light. Biorheology **25**, 471–487 (1988)
52. Guerra, T., Tiago, J., Sequeira, A.: Optimal control in blood flow simulations. Int. J. Non Linear Mech. **64**, 57–69 (2014)
53. Gijsen, F.J.H., Allanic, E., van de Vosse, F.N., Janssen, J.D.: The influence of the non-Newtonian properties of blood on the flow in large arteries: unsteady flow in a 90° curved tube. J. Biomech. **32**(6), 601–608 (1999)
54. Gregg, D.: Dynamycs of blood and lymph flow. In: Best, C., Taylor, N. (eds.) The Physiological Basis of Medical Practice. 8th edn. Williams and Wilkins, New York (1966)
55. Guyton, A.: Textbook of Medical Physiology, 8th edn. W.B. Saunders, Philadelphia, PA (1991)
56. Herschel, W.H., Bulkley, R.: Measurement of consistency as applied to rubber-benzene solutions. Proc. ASTM, Part II **26**, 621–629 (1926)
57. Huang, C., Chai, Z., Shi, B.: Non-Newtonian effect on hemodynamic characteristics of blood flow in stented cerebral aneurysm. Commun. Comput. Phys. **13**(3), 916–928 (2013)
58. Hundertmark-Zavková, A., Lukáčová-Medvidová, M.: Numerical study of shear-dependent Non-Newtonian fluids in compliant vessels. Comput. Math. Appl. **60**(3), 572–590 (2010)
59. Hughes, T.J.R., Franca, L., Balestra, M.: A new finite element method for computational fluid dynamics: V. Circumventing the Babuska-Brezzi condition: a stable Petrov-Galerkin formulation of the Stokes problem accommodating equal order interpolations. Comput. Methods Appl. Mech. Eng. **59**, 85–99 (1986)
60. Jameson, A., Schmidt, W., Turkel, E.: Numerical solutions of the Euler equations by finite volume methods using Runge-Kutta time-stepping scheme. In: AIAA 14th Fluid and Plasma Dynamics Conference, Palo Alto (1981), AIAA paper 81 - 1259 (1981)
61. Janela, J., Moura, A., Sequeira, A.: A 3D non-Newtonian fluid-structure interaction model for blood flow in arteries. J. Comput. Appl. Math. **234**(9), 2783–2791 (2010)
62. Janela, J., Moura, A., Sequeira, A.: Absorbing boundary conditions for a 3D non-Newtonian fluid - structure interaction model for blood flow in arteries. Int. J. Eng. Sci. **48**(11), 1332–1349 (2010)
63. Janela, J., Sequeira, A., Pontrelli, G., Succi, S., Ubertini, S.: Unstructured Lattice Boltzmann method for hemodynamic flows with shear-dependent viscosity. Int. J. Mod. Phys. C **21**(06), 795–811 (2010)

64. Joseph, D.D.: Fluid Dynamics of Viscoelastic Liquids. Springer, Berlin (1990)
65. Keener, J., Sneyd, J.: Mathematical Physiology. II: Systems Physiology, 2nd edn. Springer, Berlin (2008)
66. Key, N., Makris, M., O'Shaughnessy, D., Lillicrap, D. (eds.): Practical Hemostasis and Thrombosis, 2nd edn. Wiley-Blackwell, Hoboken (2009)
67. Kim, S., Cho, Y.I., Jeon, A.H., Hogenauer, B., Kensey, K.R.: A new method for blood viscosity measurement. J. Non-Newtonian Fluid Mech. **94**, 47–56 (2000)
68. Kim, Y.H., VandeVord, P.J., Lee, J.S.: Multiphase non-Newtonian effects on pulsatile hemodynamics in a coronary artery. Int. J. Numer. Methods Fluids **58**(7), 803–825 (2008)
69. King, M.R., Hammer, D.A.: Multiparticle adhesive dynamics: hydrodynamic recruitment of rolling leukocytes. PNAS **98**(26), 14919–14924 (2001)
70. Lee, B-K., Xue, S., Nam, J., Lim, H., Shin, S.: Determination of the blood viscosity and yield stress with a pressure-scanning capillary hemorheometer using constitutive models. Korea-Aust. Rheol. J. **23**(1), 1–6 (2011)
71. Leuprecht, A., Perktold, K.: Computer simulation of non-Newtonian effects of blood flow in large arteries. Comp. Methods Biomech. Biomech. Eng. **4**, 149–163 (2001)
72. Lichtman, M.A.: Rheology of leukocytes, leukocyte suspensions, and blood in leukemia. Possible relationship to clinical manifestations. J. Clin. Invest. **52**(2), 350–358 (1971)
73. Liepsch, D., Moravec, S.: Pulsatile flow of non-Newtonian fluid in distensible models of human arteries. Biorheology **21**, 571–586 (1984)
74. Liu, B., Tang, D.: Non-Newtonian effects on the wall shear stress of the blood flow in stenotic right coronary arteries. Int. Conf. Comput. Exp. Eng. Sci. **17**(2), 55–60 (2011)
75. Lopez, L., Duck, I.M., Hunt, W.A.: On the shape of the erythrocyte. Biophys J. **8**(11), 1228–1235 (1968)
76. Lowe, G.D.O. (ed.): Clinical Blood Rheology, vols. I and II. CRC Press, Boca Raton, FL (1998)
77. Lucius, M., Stolz, J.F.: Importance of erythrocyte aggregation on the viscoelastic and thixotropic properties of blood. Clin. Hemorheol. **7**, 63–70 (1987)
78. Mandal, P.K.: An unsteady analysis of Non-Newtonian blood flow through tapered arteries with a stenosis. Int. J. Non Linear Mech. **40**(1), 151–164 (2005)
79. Mao, S.S., Ahmadi, N., Shah, B., Beckmann, D., Chen, A., Ngo, L., Flores, F.R., Gao, Y.I., Budoff, M.J.: Normal thoracic aorta diameter on cardiac computed tomography in healthy asymptomatic adult; Impact of age and gender. Acad. Radiol. **15**, 827–834 (2008)
80. Marder, V.J., Aird, W.C., Bennett, J.S., Schulman. S., White, G.C. II (eds.): Hemostasis and Thrombosis: Basic Principles and Clinical Practice, 6th edn. Lippincott Williams & Wilkins, Wolters Kluwer, Philadelphia (2013)
81. Maxwell, J.C.: On the dynamical theory of gases. Philos. Trans. R. Soc. Lond. A **157**, 26–78 (1866)
82. McDonald, D.A.: Blood Flow in Arteries, 2nd edn. The Camelot Press Ltd., Southampton, Great Britain (1974)
83. Merrill, E.W.: Rheology of blood. Physiol. Rev. **49**(4), 863–888 (1969)
84. Merrill, E.W., Gilliland, E.R., Cokelet, G.R., Shin, H., Britten, A., Wells, R.E.: Rheology of human blood, near and at zero flow. Effects of temperature and hematocrit level. Biophys. J. **3**, 199–213 (1963)
85. Merrill, E.W., Cokelet, G.R., Britten, A., Wells, R.E.: Non-Newtonian rheology of human blood. Effect of fibrinogen deduced by subtraction. Circ. Res. **13**, 48–55 (1963)
86. Merrill, E.W., Margetts, W.G., Cokelet, G.C., Gilliland, E.R.: The Casson equation and rheology of the blood near shear zero. In: Copley, A.L. (ed.) Proceedings Fourth International Congress on Rheology, Part 4, pp. 135–143. New York, Interscience (1965)
87. Molla, M.M., Paul, M.C.: LES of non-Newtonian physiological blood flow in a model of arterial stenosis. Med. Eng. Phys. **34**(8), 1079–1087 (2012)
88. Moller, P.C.F., Mewis, J., Bonn, D.: Yield stress and thixotropy: on the difficulty of measuring yield stress in practice. Soft Matter **2**, 274–288 (2006)

89. Morris, C.L., Rucknagel, D.L., Shukla, R., Gruppo, R.A., Smith, C.M., Blackshear Jr., P.: Evaluation of the yield stress of normal blood as a function of fibrinogen concentration and hematocrit. Microvasc. Res. **37**(3), 323–338 (1989)
90. Nandakumar, N., Sahu, K.C., Anand, M.: Pulsatile flow of a shear-thinning model for blood through a two-dimensional stenosed channel. Eur. J. Mech. B. Fluids **49**, 29–35 (2015)
91. Neofytou, P.: Comparison of blood rheological models for physiological flow simulation. Biorheology **41**(6), 693–714 (2004)
92. Nguyen, Q.D., Boger, D.V.: Measuring the flow properties of yield stress fluids. Annu. Rev. **24**, 47–88 (1992)
93. Osterloch, K., Gaehtgens, P., Pries, A.R.: Determination of microvascular flow patternformation in vivo. Am. J. Physiol. **278**, H1142–H1152 (2000)
94. Ottensen, J.T., Olufsen, M.S., Larsen, J.K.: Applied Mathematical Models in Human Physiology. SIAM Monographs on Mathematical Modeling and Computation SIAM, Philadelphia (2004)
95. Owens, R.G.: A new microstructure-based constitutive model for human blood. J. Non - Newtonian Fluid Mech. **14**, 57–70 (2006)
96. Pearson, M.J., Lipowsky, H.H.: Influence of erythrocyte aggregation on leukocyte margination and adhesion in postcapillary venules of rat mesentery. Am. J. Physiol. **279**, H1460–H1471 (2000)
97. Perktold, K., Hilbert, D.: Numerical solution of pulsatile flow in a carotid bifurcation. J. Biomed. Eng. **8**, 193–199 (1986)
98. Perktold, K., Peter, R.: Numerical 3D-simulation of pulsatile wall shear stress in an arterial T-bifurcation model. J. Biomed. Eng. **12**, 2–12 (1990)
99. Perktold, K., Resh, M., Peter, R.O.: Three-dimensional numerical analysis of pulsatile blood flow and wall shear stress in the carotid artery bifurcation. J. Biomech. **24**, 409–420 (1991)
100. Perktold, K., Rappitsch, G.: Computer simulation of local blood flow and vessel mechanics in a compliant carotid artery bifurcation model. J. Biomech. **28**, 845–856 (1995)
101. Popel, A.S., Johnson, P.C.: Microcirculation and hemorheology. Annu. Rev. Fluid Mech. **37**, 43–69 (2005)
102. Prager, W.: Introduction to Mechanics of Continua. Dover Phoenix Edition, New York (1961)
103. Quarteroni, A., Saleri, F., Veneziani, A.: Factorization methods for the numerical approximation of the Navier-Stokes equations. Comput. Methods Appl. Mech. Eng. **188**, 505–526 (2000)
104. Quarteroni, A., Veneziani, A., Vergara, C.: Geometric multiscale modeling of the cardiovascular system, between theory and practice. Comput. Methods Appl. Mech. Eng. **302**, 193–252 (2016)
105. Quemada, D.: Rheology of concentrated disperse systems III. General features of the proposed non-Newtonian model. Comparison with experimental data. Rheol. Acta **17**, 643–653 (1978)
106. Ramalho, S., Moura, A.B., Gambaruto, A.M., Sequeira, A.: Influence of blood rheology and outflow boundary conditions in numerical simulations of cerebral aneurysms. In: Mathematical Methods and Models in Biomedicine. Lecture Notes on Mathematical Modelling in the Life Sciences, pp. 149–175. Springer, New York (2013)
107. Rajagopal, K.R., Srinivasa, A.R.: A thermodynamic frame work for rate-type fluid models. J. Non-Newtonian Fluid Mech. **80**, 207–227 (2000)
108. Robertson, A.M., Sequeira, A., Kameneva, M.V.: Hemorheology. In: Galdi, G.P., Rannacher, R., Robertson, A.M., Turek, S. (eds.) Hemodynamical Flows: Modeling, Analysis and Simulation. (Oberwolfach Seminars), vol. 37, pp. 63–120. Birkhäuser Verlag, Basel (2008)
109. Robertson, A.M., Sequeira, A., Owens, R.G.: Hemorheology. In: Formaggia, L., Quarteroni, A., Veneziani, A. (eds.) Cardiovascular Mathematics. Modeling and Simulation of the Circulatory System, vol. 1. Springer, Berlin (2009), pp. 211–242
110. Roco, M.C. (ed.): Particulate Two-Phase Flow. Series in Chemical Engineering. Butterworth-Heinemann Publisher, London (1993)
111. Schmid-Schönbein, H., Wells, R.E.: Fluid drop-like transition of erythrocytes under shear. Science **165**, 288–291 (1969)

112. Schmid-Schönbein, H., Wells, R.E.: Rheological properties of human erythrocytes and their influence upon anomalous viscosity of blood. Physiol. Rev. **63**, 147–219 (1971)
113. Schmid-Schönbein, H., Barroso-Aranda, J., Chavez-Chavez, R.: Microvascular leukocyte kinetics in the flow state. In: Boccalon, H. (ed.) Vascular Medicine, pp. 349–352. Elsevier, Amsterdam (1993)
114. Scott-Blair, G.W.: An equation for the flow of blood, plasma and serum through glass capillaries. Nature **183**, 613–614 (1959)
115. Secomb, T.W.: Mechanics and computational simulation of blood flow in microvessels. Med. Eng. Phys. **33**, 800–804 (2010)
116. Sequeira, A., Artoli, A.M., Silva-Herdade, A.S., Saldanha, C.: Leukocytes dynamics in microcirculation under shear-thinning blood flow. Comput. Math. Appl. **58**(5), 1035–1044 (2009)
117. Sequeira, A., Bodnár, T.: Blood coagulation simulations using a viscoelastic flow model. Math. Model. Nat. Phenom. **9**(6), 34–45 (2014)
118. Serrin, J.: Mathematical principles of classical fluid mechanics. In: Flugge, S., Truesdell, C. (eds.) Handbuch der Physik, vol. VIII/I. Springer, Berlin (1959)
119. Skalak, R., Tozeren, A., Zarda, R., Chein, S.: Strain energy function of red blood cell membranes. Biophys. J. **13**(3), 245–264 (1973)
120. Silverthorn, D.U.: Human Physiology. An Integrated Approach, 7th edn. Prentice Hall, Upper Saddle River, NJ (2015)
121. Thiriet, M.: Biology and Mechanics of Blood Flows. Part I: Biology. CRM Series in Mathematical Physics. Springer, Berlin (2008)
122. Thiriet, M.: Biology and Mechanics of Blood Flows. Part II: Mechanics and Medical Aspects. CRM Series in Mathematical Physics. Springer, Berlin (2008)
123. Thiriet, M., Parker, K.H.: Physiology and pathology of the cardiovascular system: a physical perspective. In: Formaggia, L., Quarteroni, A., Veneziani, A. (eds.) Cardiovascular Mathematics. Modeling and Simulation of the Circulatory System, vol. 1, pp. 1–46 Springer, Berlin (2009)
124. Thurston, G.B.: Viscoelasticity of human blood. Biophys. J. **12**, 1205–1217 (1972)
125. Thurston, G.B.: Frequency and shear rate dependence of viscoelasticity of human blood. Biorheology **10**, 375–381 (1973)
126. Thurston, G.B.: Elastic effects in pulsatile blood flow. Microvasc. Res. **9**, 145–157 (1975)
127. Thurston, G.B.: Non-Newtonian viscosity of human blood: flow induced changes in microstructure. Biorheology **31**(2), 179–192 (1994)
128. Thurston, G.B.: Viscoelastic properties of blood and blood analogs. Adv. Hemodyn. Hemorheol. **1**, 1–30 (1996)
129. Toksvang, L.N., Berg, R.M.G.: Using a classic paper by Robin Fåhraeus and Torsten Lindqvist to teach basic hemorheology. Adv. Physiol. Educ. **37**(2), 129–133 (2013)
130. Vierendeels, J., Riemslagh, K., Dick, E.: A multi-grid semi-implicit line-method for viscous incompressible and low-Mach-number flows on high aspect ratio grids. J. Comput. Phys. **154**, 310–344 (1999)
131. Vlastos, G., Lerche, D., Koch, B.: The superposition of steady on oscillatory shear and its effect on the viscoelasticity of human blood and a blood-like model fluid. Biorheology **34**, 19–36 (1997)
132. Yeleswarapu, K.K., Kameneva, M.V., Rajagopal, K.R., Antaki, J.F.: The flow of blood in tubes: theory and experiment. Mech. Res. Commun. **25**(3), 257–262 (1998)
133. Walburn, F.J., Schneck, D.J.: A constitutive equation for whole human blood. Biorheology **13**, 201–210 (1976)
134. Zhang, J., Johnson, P.C., Popel, A.S.: Effects of erythrocyte deformability and aggregation on the cell free layer and apparent viscosity of microscopic blood flows. Microvasc. Res. **77**(3), 265–272 (2009)
135. Zwaal, R.F., Hemker, H.C.: Blood Coagulation. Elsevier Science Publishers, North Holland (1986)